T-AM-Sym1 BACTERIORHODOPSIN STRUCTURE: IMPLICATIONS FOR THE FOLDING OF MEMBRANE PROTEINS.
D.M. Engelman, Department of Molecular Biophysics and Biochemistry, Yale University, Box 6666, New Haven, CT. 06511

Structural studies on bacteriorhodopsin have established that the membrane spanning portion of the structure consists of a bundle of 7 helices. Energy calculations using the amino acid sequence predict 7 alpha helical segments which would be stable as membrane-spanning elements. Similar calculations on a variety of other membrane proteins show the presence of sequences which would also be stable as transmembrane helices. It appears a reasonable hypothesis that helical structures spanning the membrane are folding intermediates in the assembly of globular membrane proteins, and that the helices may be retained in the final, folded structure in many cases. The finding from neutron scattering studies that the polar surfaces of the helices in bacteriorhodopsin come together in the assembly of the helical bundle suggest that, once formed, membrane helices may assemble in response to polar interactions, forming a folded, functional membrane protein. Theoretical and experimental results on bacteriorhodopsin and other membrane proteins will be discussed in the context of the insertion and folding of membrane proteins.

T-AM-Sym2 **THOUGHTS ON THE VARIETY OF INTEGRAL MEMBRANE PROTEIN STRUCTURES**
S. J. Singer, **Dept. of Biology, UCSD, La Jolla, CA**

T-AM-Sym3 **STRUCTURE AND TRANSITIONAL STATES OF GAP JUNCTION CHANNELS**
P. N. T. Unwin, **Dept. of Structural Biology, Stanford University, Stanford, CA.**

T-AM-Sym4 **RECENT PROGRESS IN STRUCTURE AND FUNCTION ANALYSIS OF PORIN**
J. P. Rosenbusch, European Molecular Biology Lab., 6900 Heidelberg, FRG.

T-AM-Sym5 **HIGH RESOLUTION STRUCTURE OF PROTEIN AND LIPID IN THE PURPLE MEMBRANE**
D. Agard, UC Medical Center, San Francisco, CA.

T-AM-Min1 Base Sequence and Helix Structure Variation in B- and A-DNA
Richard E. Dickerson, Molecular Biology Institute, University of California at Los Angeles, Los Angeles, CA 90024, U.S.A.

The observed propeller twist in base pairs of crystalline double-helical DNA oligomers improves the stacking overlap along each individual helix strand. But as proposed by Calladine (J. Mol. Biol. (1982) 161, 343-352) it also leads to clash or steric hindrance between purines at adjacent base pairs on opposite strands of the helix. This clash can be relieved by (1) decreasing the local helix twist angle between base pairs, (2) opening up the roll angle between base pairs on the side on which the clash occurs, (3) separating purines by sliding base pairs along their long axes so the purines are partially pulled out of the stack (leading to symmetrical alterations in main chain torsion angle δ at the two ends of the base pair), and (4) flattening the propeller twist of the offending base pairs. Simple sum functions, Σ_1 through Σ_4, are defined, by which the expected local variation in helix twist, base roll angle, torsion angle δ and propeller twist may be calculated from base sequence. All four functions are quite successful in predicting the behavior of B-DNA. Only the helix twist and base roll functions are applicable to A-DNA, and the helix twist function begins to fail for an A-helical RNA/DNA hybrid. Within these limits, the sequence-derived sum functions match the observed helix parameter variation quite closely, with correlation coefficients greater than 0.900 in nearly all cases. Implications of this sequence-derived helix parameter variation for repressor-operator interactions are considered.

T-AM-Min2 ONE- AND TWO-DIMENSIONAL NMR STUDIES OF DNA STRUCTURES.
D.R. Kearns, N. Assa-Munt, R. Behling, W.A. Denny, J. Feigon, J. Granot, W. Leupin and P. Mirau. Chemistry Department, University of California-San Diego, La Jolla, CA 92093

We have used a variety of NMR relaxation techniques to investigate the structures of DNA molecules in solution. From 2D NOSEY experiments we can immediately identify most of the short interproton distances in the molecule. To obtain semi-quantitative or quantitative information on distances, appropriate selective and bi-selective relaxation measurements are carried out. COSY experiments and 2D J-coupling experiments provide additional information useful in the assignments of the spectra. Application of the above set of techniques to an investigation of a number of DNA, including poly(dA-dT), poly(dG-dC), poly(dI-dC) and several DNA decamers permitted us to identify a number of structural features in each molecule. For poly(dA-dT), a molecule we have studied in some detail, we find that the AH2 protons in adjacent A•T base pairs are surprisingly close together (relative to standard B-DNA). These and other examples will be used to illustrate the use of NMR techniques in the elucidation of both structural and dynamic properties of DNA.

T-AM-Min3 LEFT-HANDED DNA HELICES, SUPERCOILING, AND THE B-Z JUNCTION
Robert D. Wells, Department of Biochemistry, School of Medicine and Dentistry, University of Alabama in Birmingham, Birmingham, Alabama 35294

Biological and physical studies on recombinant plasmids and restriction fragments containing tracts of (dC-dG) sequences which are 58, 32, 26, and 10 bp in length reveal the following: A) Left-handed Z-DNA can neighbor right-handed regions of DNA in close proximity on the same chain (1-7). B) Negative supercoiling (density greater than 0.072 is sufficient to convert the 58 bp (dC-dG) regions in pRW751 into a left-handed structure under physiological ionic conditions (200mM NaCl). Thus, left-handed DNA probably exists in vivo (6). C) Single-strand specific nucleases recognize and cleave aberrant structural features at the B-Z junctions (6,8). D) The B-Z junction is very short (several bp) as judged by ^{31}P-NMR, Raman spectroscopy, extent of relaxation of supercoils, and the sharpness of the products of single-strand specific nucleases (1-7). E) The left-handed conformation perturbs the right-handed backbone structure neighboring the B-Z junction for 3-4 helical turns as judged by Raman spectroscopy (5). F) (dC-dG) sequences exist in a family of left-handed conformations as stabilized by different conditions. Furthermore, spectroscopically identifiable conformational intermediates exist between the B and Z structures (7). G) A cloned segment of immunoglobulin gene containing $(dT\text{-}dG)_{31}\cdot(dC\text{-}dA)_{31}$ adopts a left-handed conformation under the influence of negative supercoiling (8). Also, the AAF-reacted polymer is left-handed in high salt solutions (4). H) The stabilizing effect of methylation on the Z-form in fragments and plasmids approximately offsets the free energy contributions of the B/Z junctions (9). I) The (dC-dG) tracts are specifically and highly susceptible to suffer deletions in vivo. Also, these tracts seem to enhance rec A mediated recombination (1,2).

1. Klysik, Stirdivant, Larson, Hart, and Wells, Nature 290, 627-677 (1981).
2. Klysik, Stirdivant, and Wells, J. Biol. Chem., 257, 10152-10158 (1982).
3. Stirdivant, Klysik, and Wells, J. Biol. Chem., 257, 10159-10165 (1982).
4. Wells, Miglietta, Klysik, Larson, Stirdivant, and Zacharias, J. Biol. Chem., 257, 10166-10171 (1982).
5. Wartell, Klysik, Hillen, and Wells, P.N.A.S., 79, 2549-2553 (1982).
6. Singleton, Klysik, Stirdivant, and Wells, Nature 299, 312-316 (1982).
7. Zacharias, Larson, Klysik, Stirdivant, and Wells, J. Biol. Chem. 257, 2775-2782 (1982).
8. Singleton and Wells, unpublished work.
9. Klysik, Stirdivant, Singleton, Zacharias, and Wells, J. Mol. Biol. in the press (1982).

T-AM-Min4 THEORETICAL ANALYSES OF SUPERCOILED DNA, Craig J. Benham, Mathematics Department, University of Kentucky, Lexington, KY 40506.

A closed circular molecule of duplex DNA has a fixed value of its linking number Lk. Deviations of Lk from its relaxed value impose stresses on the duplex, which responds by bending and/or altering its total molecular twist so as to minimize its conformational free energy consistent with constraints. Results from two theoretical treatments of the behavior of stressed molecules will be presented. First, the large-scale tertiary structure of superhelical molecules will be analyzed. Here the topological constraint imposed by the constancy of Lk is partitioned between bending and smooth torsional deformations so as to minimize the elastic strain energy. At high superhelix densities alterations in total molecular twist may involve local transition to conformations having different unstressed twist rates as well as smooth elastic strain of the resulting structures. The second analysis treats stress-induced transitions in secondary structure and their competition in torsionally deformed DNA. The alternative conformations include Z-form, cruciforms, and locally denatured regions. These results suggest that the regulations of DNA superhelicity can orchestrate an intricately interacting repertoire of events.

T-AM-A1 BINDING OF AN INDOLE DERIVATIVE TO MICELLES AS QUANTIFIED BY PHASE SENSITIVE DETECTION OF FLUORESCENCE by Susan Keating and Joseph R. Lakowicz, University of Maryland, School of Medicine, Department of Biological Chemistry, Baltimore, Maryland 21201.

The association of ligands with proteins and membranes occurs widely in biological systems, and the analysis of such reactions is widespread in biochemical research. We present a new application of phase sensitive detection of fluorescence, this being the quantitation of an association reaction. As a model we studied the binding of 6-In-11 (11-(3-hexyl-1-indolyl)undecyltrimethyl ammonium bromide) to micelles of HDTBr(hexadecyltrimethylammonium bromide), a system described previously by Turro and co-workers (Photochem. Photobiol. 31, 527-532, 1980). Upon binding to the micelles the lifetime of 6-In-11 increases from 7.3 to 17.3 ns. By phase sensitive detection of fluorescence one may suppress the emission from either form (free or bound) of 6-In-11. Then, the signal is proportional to the concentration of 6-In-11 in the other form (bound or free). In combination with the measured lifetimes the phase sensitive intensities permit the concentration of each form to be determined. As the concentration of HDTBr was increased the phase sensitive intensities revealed that the concentration free 6-In-11 decreased cooperatively, as expected for micelle formation by HDTBr. This method can be applied generally to any association reaction where one of the species is fluorescent, and where the lifetime of the free and bound forms are different. Fortunately, these are common occurrences, and lifetime differences of 1 nanosecond are adequate to resolve the individual species. An advantage of this method is that the association reaction may be quantified without physical separation of the individual species.

T-AM-A2 PHASE TRANSITIONS IN PHOSPHOLIPID MONOLAYERS BY LATERAL DIFFUSION. M. Seul, R. M. Weis & H. M. McConnell; Stauffer Laboratory for Physical Chemistry, Stanford Univ., Stanford CA 94305.

A monomolecular phospholipid layer was transferred at a given surface pressure and temperature from an air-water interface to a planar substrate treated with octadecyltrichlorosilane. Substrates used were glass, quartz, and silicon.[1] Monolayers containing the fluorescent lipid probe, NBD-PE (1 mol%), were examined by epifluorescence microscopy and the lateral diffusion was measured using periodic pattern fluorescence photobleaching recovery.[2] The measurements were performed as a function of temperature. Data are presented for two specific systems, namely DMPC on glass and DPPC on silicon. Characteristic changes of the diffusion coefficient (D) are observed as a function of temperature, indicative of thermotropic phase transitions for the fully hydrated monolayers. For hydrated DMPC on glass, D increased two orders of magnitude from 10^{-10} cm^2/sec in a transition centered at 21°C. For hydrated DPPC on silicon two transitions occur at temperatures corresponding to well-known transitions in multibilayers of this material at 35°C ($L_{\beta'}$-$P_{\beta'}$) as well as 39.5°C ($P_{\beta'}$-L_{α}). There is evidence for an additional transition at 27°C which is less pronounced and is only observed on heating runs. No transitions were found up to 55°C when the system was transferred to an atmosphere of water-saturated helium. While the structural nature of the various phases remains to be characterized, the transition at 35°C does suggest the existence of a $P_{\beta'}$ phase in monolayers, emphasizing the weak interlayer-coupling in bilayer systems.

[1]Weis et al (1982) J. Biol. Chem., 257, 6440-6445.
[2]Smith and McConnell (1978) PNAS USA, 78, 2759-2763.

T-AM-A3 ELECTROSTATIC FORCES CONTROLLING SOLUTE PERMEATION THROUGH LECITHIN BILAYERS.

John Bramhall, Microbiology & Immunology Dept., UCLA Medical School, Los Angeles, California 90024

Experiments with the fluorescent dyes 6-carboxyfluorescein (6-CF) and 8-anilino-1-naphthalene sulfonate (ANS) demonstrate that the rate of efflux of these anionic dyes can be dramatically stimulated by the presence of agents, such as gramicidin, which increase specific membrane cation permeability. Measurements of the temperature dependence of the rate of ANS translocation across lecithin (DPPC) vesicle membranes indicate that there is a sharp rate maximum at a temperature coinciding with the phase transition point (Tc) of the lipid. When these vesicles are preincubated with gramicidin, not only does the rate of anionic dye translocation increase at all temperatures, but there is also no longer a rate maximum at Tc. Instead, the translocation kinetics appear very similar to those observed for electrically neutral dyes. The temperature dependence for ANS translocation is thus a reflection of the temperature dependence of sodium ion permeation across the bilayer. Since the intrinsic permeation rate of ANS and 6-CF across a lecithin bilayer, measured under exchange-diffusion conditions, is greater than the permeation rate for sodium ions, the rate of leakage of such dyes (and similar solutes) will always reflect the rate of leakage of sodium. It is commonly assumed that a dye such as 6-CF is "too polar" to pass through a lipid bilayer. In fact, 6-CF is perfectly capable of rapid transit across lecithin membranes, the true controlling force is electrostatic in nature.

T-AM-A4 FLUORESCENCE PROBE STUDIES OF LECITHIN-BILE SALT MIXED MICELLES. C.H. Spink and Frank Phelan, Chemistry Department, State University of New York, Cortland, NY 13045.

The fluorescence quantum yields and vibronic band intensities of pyrene monomers were studied as probes of the behavior of mixed micelles of dipalmitoylphosphatidylcholine (DPPC) and bile salts. Micelles of taurodeoxycholate (TDC) and DPPC produced a marked increase in fluorescent quantum yield for micromolar quantities of pyrene in the micelles as the mole ratio of TDC/DPPC increased from about 1/1 to 2/1. Above this ratio the yield increased much more slowly. The intensities of vibronic bands of pyrene at 383 nm (III) and at 372 nm (I) were also studied in the mixed micelles. Again the TDC-DPPC micelles caused the III-I ratios of pyrene (a measure of polarity of the environment) to increase rather sharply up to a 2/1 ratio. The variations in quantum yield and III-I ratios also were found to depend on the total lipid content. With taurocholate (TC) mixed micelles with DPPC the behavior was similar to TDC-DPPC micelles except that the onset of change in the pyrene spectra occurred at higher mole ratios. The results show trends that are consistent with previous scanning calorimetry data which indicate a change in micellar structure at higher mole ratios.

T-AM-A5 GENERAL ANALYSIS OF TIME RESOLVED FLUORESCENCE ANISOTROPY IN MODEL MEMBRANES

W. van der Meer (Leiden), M. Ameloot (Diepenbeek), W. Herreman, H. Pottel (Kortrijk) and H. Schröder (Konstanz) (Intr. by A.A. Lamola)
c/o Interdisciplinary Research Center, K.U.Leuven, B-8500 Kortrijk, Belgium.

Our analysis is general in the sense that it is not necessary to specify the orientational distribution. It is based on a solution of the rotational diffusion problem for a rodlike probe in a membrane, in terms of two orientational order parameters and one diffusion constant.
Nanosecond Fluorescence Anisotropy (FA) studies using 1,6-diphenyl-1,3,5-hexatriene (DPH) as a probe in model membranes are very well described by this theory.
Our conclusions:

1. One exponential plus a constant gives a poor fit for the FA.
2. The decay of the total DPH fluorescence must be described by more than one exponential.
3. It is possible to estimate the orientational distribution for the probe. This deviates considerably from the cone model distribution, because it exhibits a secondary maximum in a direction perpendicular to the membrane normal.

Our results indicate that DPH diffuses within the fluorescence lifetime from a position between the hydrocarbon chains towards the plane in the middle of the bilayer and back again. In a highly ordered membrane this type of motion is very rare and even in a disordered membrane the most probable orientation is close to the membrane normal.

T-AM-A6 FLUORESCENCE POLARIZATION ORDER PARAMETERS AND PHASE TRANSITIONS IN LIPIDS AND LIPOPROTEINS. Elliott Berlin and Eduardo Sainz, Lipid Nutrition Laboratory, BHNRC, U.S. Dept. of Agriculture, Beltsville, MD 20705

Phase transitions in sonicated lipid dispersions of triglycerides (TG), cholesteryl esters (CE), or phospholipids were observed in fluorescence depolarization measurements with DPH. Transition to an isotropic liquid was detected in a novel way by noting the temperature, $t_{.08}$, at which r_s, the steady state anisotropy value was 0.08 corresponding to a zero value for S, the order parameter, in the theoretical equation of Van Blitterswijk, et al (BBA 644 (1981) 523). Good agreement was noted between results by this method and by differential scanning calorimetry (DSC) with saturated TG. Temperatures, $t_{.08}$, were 36, 45, and 52.5°C for 16:0, 17:0, and 18:0 containing TG, respectively; corresponding DSC fusion temperatures were 41, 45, and 52°C. Trielaidin (trans 18:1) melted at 38°C (DSC) and exhibited $t_{.08}$ = 37.5°C. Similar agreement was noted in a phospholipid, with distearoyl lecithin liposomes melting at 58°C (DSC) and displaying $t_{.08}$ = 59°C. In contrast $r_s > 0.08$ was observed with cholesteryl esters of 12:0, 14:0, 16:0 18:0 and 18:1 fatty acids at temperatures above their DSC melting points. The decreased probe freedom characteristic of the cholesteryl esters becomes significant as more CE is added to TG + CE mixtures. This difference in the rotational movement of DPH in TG and CE systems may explain the inverse relation between $t_{.08}$ and TG/CE ratios in plasma very low density lipoproteins and the higher $t_{.08}$ values observed in the more dense lipoprotein fractions which contain significantly more CE and less TG.

T-AM-A7 PHOTOBLEACHING RECOVERY STUDIES OF T-INDEPENDENT ANTIGEN MOBILITY ON ANTIBODY-BEARING LIPOSOMES, James S. Peacock and B. George Barisas, Department of Chemistry, Colorado State University, Fort Collins, Colorado 80523.

Palmitate-conjugated MOPC-315, anti-DNP IgA, was incorporated into 15 μm diameter liposomes prepared from phosphatidylcholine, cholesterol and cardiolipin (2:2:1). At 37°C, liposome-bound tetramethylrhodamine isothiocyanate (TRITC)-labeled anti-DNP antibody diffuses at 1.4×10^{-8} cm^2 sec^{-1}, a rate comparable to that observed for the phospholipid analog diI-C_{18}-(3). Both substances exhibit complete fluorescence recovery after bleaching. The binding of TRITC-conjugates of the antigens DNP-polymerized flagellin (DNP-POL) and DNP-dextran (DNP-DEX) to liposomes bearing non-fluorescent palmitoyl-MOPC 315 was then examined. The diffusion constants observed for bound antigens decrease monotonically with increased antigen dose and epitope density. For low epitope density antigens, the DNP-DEX and DNP-POL complexes are almost completely mobile. At higher epitope densities liposomes bearing 150,000 Ig molecules exhibit a fraction of bound antigen which is immobile on the time scale of the experiment. This fraction is dependent on antigen concentration and epitope density. At 10 μg/ml $DNP_{2.2}$-POL diffuses at 1.0×10^{-9} cm^2 sec^{-1} and 10% of the bound antigen is immobile. The immobile fraction increases to 31.5% for $DNP_{4.0}$-POL at 30 μg/ml though D for mobile antigen falls only to 5.0×10^{-10} cm^2 sec^{-1}. $DNP_{3.2}$-DEX at 10 μg/ml yields an immobile fraction of 14.3% which increases to 47.6% for $DNP_{8.0}$-DEX at 100 μg/ml. Under comparable conditions liposomes bearing 70,000 Ig molecules exhibit antigen immobile fractions of about half the above values. The observed immobile fractions may represent formation of a two-dimensional gel phase of antigen-immunoglobulin aggregates. Supported by NSF PCM 81-11385 and NIH RCDA AI-00506.

T-AM-A8 TIME-RESOLVED FLUORESCENCE STUDIES OF THE SINGLE TRYPTOPHAN OF PORCINE PHOSPHOLIPASE A_2 IN SOLUTION AND BOUND TO A LIPID-WATER INTERFACE. Richard Ludescher, Johannes Volwerk, Bruce Hudson, Patricia Jost and Gerard de Haas, Institute of Molecular Biology, University of Oregon, Eugene, OR 97403 and Biochemical Laboratory, State University of Utrecht, Utrecht, The Netherlands

Pancreatic phospholipase A_2(PLA_2) catalyses the hydrolysis of the fatty acid ester bond at the 2 position of 3-sn-phosphoglycerides organized into lipid-water interfaces at a rate 3 to 4 orders of magnitude faster than for monomeric substrates. Binding of the enzyme to organized substrate (analogs) has dramatic effects on the fluorescence of the single tryptophan: the emission is blue shifted and narrows and the quantum yield increases ~3-fold, all indicative of transfer to a hydrophobic environment. The enzyme is secreted by the pancreas in the form of a zymogen which does not bind to neutral interfaces because the N-terminal α-NH_2 group, which triggers formation of the interfacial lipid binding site, is blocked by an extra heptapeptide. Time-resolved fluorescence lifetime and anisotropy decays of the tryptophan in both forms of the enzyme free in solution and in the presence of organized lipids have been collected. The tryptophan has multiple lifetimes in all situations, but the increase in quantum yield is not mirrored by a comparable increase in lifetimes. The anisotropy decays are sensitive to two motions, a slow decay compatible with predicted particle rotational correlation times (τ_c) and a fast decay ($\tau_c < 1$ ns). The amplitude of the fast decay decreases when PLA_2 binds to the lipid-water interface indicating that the extent of the tryptophan motion is decreased by the lipid. This limitation of the tryptophan motion is possibly due to interdigitation of the aromatic side chain with the lipid acyl chains. (This work is supported by NIH Grants GM 26536 and GM 25698. R.L. is an NIH pre-doctoral trainee.)

T-AM-A9 DANSYL-LYSINE AND DANSYL-AMINOBUTYRATE AS FLUORESCENT MEMBRANE PROBES. Gillian M.K. Humphries and John P. Lovejoy, Institute for Medical Research, San Jose, CA 95128.

On examination of single cell suspensions prepared from organs normally concerned with providing immunity (spleen, etc.), we find that live, nucleated cells are able to distinguish between dansyl-γ-aminobutyrate (DB) and ϵ-dansyl-lysine (DL). Their membranes are stained by DB but not DL (DB^+DL^- cells). There are exceptions: many human leukemic cells and mouse bone-marrow (hemopoietic?) cells are DB^+DL^+. Furthermore, when cells die (as determined by ability to take up trypan blue) they become DB^+DL^+. Thus, DL has the same selectivity amongst these cells as reported by others for merocyanin 540. In addition, we find that a $DB^+DL^- \rightarrow DB^+DL^+$ change of state is induced in living cells under certain circumstances, e.g. mouse peritoneal exudate cells after periods of adherence to glass etc., spleen cells on heating or PEG treatment.

In an attempt to discover the basis for staining selectivity and the possible significance of changes in state, we have been engaged in two types of study: (a) concerning the properties of DL and DB, particularly their interactions with phospholipid-cholesterol model membranes; (b) concerning conditions under which changes in cell-staining state occur, and relationship to function.

DL has the structure of DB with an additional $—CH_2—CH(NH_3^+)—$ moiety inserted. Cells and liposomes which are DB^+DL^+ always stain slightly more intensely with DL than with DB (we measure the partition coefficients of DL and DB into DMPC as ~10 and ~8 respectively). Extensive variation of composition with respect to cholesterol, phospholipids and charged lipids has failed to yield DB^+DL^- liposomes. The property of many living cells which enables them to resist staining with DL remains unknown at this time. (AI 17525)

T-AM-A10 RAPID LATERAL DIFFUSION OF A DIFFERENTIATION ANTIGEN WITHIN A LOCALIZED SURFACE DOMAIN OF GUINEA PIG SPERM. Dennis E. Koppel*, Diana Gold Myles‡, and Paul Primakoff‡, Departments of Biochemistry* and Physiology‡, University of Connecticut Health Center, Farmington, CT 06032

A mapping of the guinea pig sperm surface with monoclonal antibodies has revealed a surface mosaic of distinct regions with different compositions. Immunofluorescence microscopy defines five regions of surface antigen localization: the anterior head(AH), posterior head(PH), whole head(WH), posterior tail(PT), and whole tail(WT). In each of the head regions, several different protein antigens share the same localization (D.G.Myles, P.Primakoff, and A.R.Bellvé,Cell 23,433(1981); P. Primakoff and D.G.Myles, unpublished results). To approach the question of what mechanisms operate to develop and maintain this topological localization, we have begun the characterization of the lateral mobility of labeled surface antigens using the technique of fluorescence redistribution after photo-bleaching(FRAP). We report here that a surface antigen localized on the posterior tail diffuses rapidly($D = 2.5 \times 10^{-9} cm^2/sec$) and completely (> 95% recovery after bleaching) within its surface domain. This result rules out models which invoke immobilization as the way of maintaining localization of this antigen. (Supported by NIH Grants GM-23585 and HD-16580).

T-AM-A11 TIME-LAPSE VIDEO RECORDING OF INDIVIDUAL MOLECULAR MOTIONS OF LDL-RECEPTOR COMPLEX ON LIVING HUMAN FIBROBLASTS. David Gross and Watt W. Webb, School of Applied and Engineering Physics, Clark Hall, Cornell University, Ithaca, NY, 14853.

Motion of individual macromolecular complexes on the living cell surface is recorded and analyzed using a video microscopy apparatus with digital recording and storage of phase contrast and fluorescence images. Illumination of the specimen for time lapse records is controlled by a fast (1 msec) shutter to limit photobleaching. Recording, playback and subsequent image analysis (summation, subtraction, enhancement and tracking) are under interactive computer control. Two distinct advantages are apparent for this technique over fluorescence photobleaching recovery (FPR) for the study of slow diffusive or non-diffusive motion of single molecules: 1) 2-dimensional information over a large area is directly obtainable for analysis of non-diffusive or position-dependent diffusive motion and 2) putative photodamage due to high-intensity photobleaching beams is eliminated. To illustrate these points, we report observations of the motions of fluorescently-labelled LDL bound to LDL receptors on human internalization-deficient "J.D." fibroblasts (GM2408A). The fluorescence-visualized single molecule, dil-LDL, has been described previously (Barak and Webb, J. Cell Biol. 90, 595-604, 1981). Early results show dramatic, strongly-localized motion of individual probe-receptor complexes at two time scales, fast (<1 sec) and slow (10 min). Fast motion, easily seen in real time, is localized above the plane of the cell surface, presumably on membrane extensions. Slow motion, visualized by time-lapse, is localized in the plane of the cell membrane.

(Supported by grants NIGMS GM 27533, NIH-CA14454 and NSF-80-07634.)

T-AM-A12 RETROVIRUS TRANSFORMATION CHANGES EXTRINSIC RECEPTOR DIFFUSIBILITY MEASURED BY FLUORESCENCE PHOTOBLEACHING RECOVERY. W. Carley+, P. Kurtz* and W. W. Webb+, School of Applied and Engineering Physics+ and the Department of Physics*, Cornell University, Ithaca, NY 14853.

Acetyl-rhodamine-stearoylated-dextran (AcRSD) mimics a membrane receptor protein since its fatty acid moiety inserts into the membrane bilayer and its sugar polymer remains exposed to interact with all surface carbohydrates (Wolf, et al., Biochemistry 19, 3893(1980)). The lateral mobility of AcRSD has been measured on normal rat kidney cells (NRK) and on Rous sarcoma virus transformed NRK cells (Pr-NRK). On NRK cells its diffusion coefficient $D = 4$ to $10 \times 10^{-10} cm^2/sec$ with $85 \pm 15\%$ recovery at 23°C; on Pr-NRK (transformed) cells $D = 2$ to $8 \times 10^{-9} cm^2/sec$ with $40 \pm 12\%$ recovery. These differences between normal and transformed cells are not due to the increased fraction of Pr-NRK cells in mitosis because D and the percent recovery are unchanged on mitotic NRK cells while mitotic Pr-NRK cells retain the same percent recovery and D decreases only to $4 \times 10^{-10} cm^2/sec$. Transformation increases D by nearly an order of magnitude but decreases the fractional recovery significantly. The AcRSD appears uniformly distributed on both cell types. Significant cytoskeletal changes accompany transformation in these cells but as yet have not been implicated in these diffusivity changes. The significance of surface carbohydrate interactions with the synthetic receptor are estimated by stripping carbohydrates from membrane glycoproteins with endoglycosidases and aqueous phase viscous drag is estimated by assaying diffusibility in the presence of large dextran polymers. (Supported by NIH grant CA 14454C and NSF grant 8007634).

T-AM-B1 IONIC BALANCE AND VOLUME REGULATION IN SYNCYTIA. R.T. Mathias and J.L. Rae. Dept. of Physiology, Rush Medical College, Chicago, Illinois 60612.

The relationship between resting voltages, ion concentrations, active transport and volume regulation in the lens has been investigated using a variety of techniques. Because of the relatively large overall dimensions of the lens, or other syncytia, when compared to the tiny pervading intercellular space, there can be significant spatial variations in intercellular voltage and ion concentrations. Such spatial variations produce a rather complex steady state, where no ion is in electrochemical equilibrium, steady state currents circulate from surface to center of the tissue and standing circulating water flow may exist. All of these effects have been analyzed by a perturbation expansion of the field equations for water flow due to hydrostatic and osmotic pressure, and ion flux due to convection and electrodiffusion. We now have experimental data which allow estimation of most parameters in the theoretical model. For the frog lens, given the available experimental data, we predict relatively large voltage gradients (50 mV) along the intercellular clefts and smaller (5 mV) gradients in the intracellular voltage. These predictions will be compared to measurements of intracellular resting voltage and intercellular resting voltage. (Supported by NIH grants EY 03095 and EY 03282.)

T-AM-B2 ASYMMETRY IN THE PACKING OF CONNEXONS IN GAP JUNCTIONS. T.S. Baker, D.L.D. Caspar, Rosenstiel Basic Medical Sciences Research Center, Brandeis University, Waltham, MA and C. Gall, D.A. Goodenough, Harvard Medical School, Department of Anatomy, Boston, MA.

Micrographs of mouse liver gap junctions, isolated with detergents, and contrasted either with anionic or cationic negative stains have been recorded by low-irradiation methods. Our Fourier-averaged micrographs of the hexagonal junction lattice show skewed, hexameric connexons, usually with less stain at the three-fold axis than at the six indentations between the lobes of the connexon image. Following an electron dose less than normally used in microscopy, the connexon image is converted to the familiar doughnut shape, with a darkly stained center and a smooth hexagonal outline, oriented with mirror symmetry in the lattice. Differences in appearance among 25 reconstructed images from our low-irradiation micrographs of uranyl acetate stained junction specimens illustrate variation in staining of the connexon channel and the space between connexons. Comparable observations of specimens stained in different ways consistently show stain concentration at six symmetrically related sites ∿34Å from the connexon center, 8° to the right or left of the [1,1] lattice vector. The unexpected skewing of the six-lobed connexon image indicates that the pair of hexagonal membrane arrays that form the junction are not structurally identical. Since the projected image of the connexon pair itself appears mirror symmetric, each pair may consist of two, identical connexon hexamers related by local (non-crystallographic) two-fold axes in the junctional plane at the middle of the gap. The packing of the connexons on the two sides of the junction appears to be non-equivalent, although all connexons may be chemically identical.

Supported by NIH grants CA15468 (DLDC) and GM18974 (DAG).

T-AM-B3 ANALYSIS OF CELL-TO-CELL DIFFUSION KINETICS: CHANGES IN JUNCTIONAL PERMEABILITY WITHOUT ACCOMPANYING CHANGES IN SELECTIVITY. A.L. Zimmerman and B. Rose. Dept. of Physiology and Biophysics, University of Miami School of Medicine, Miami, FL. 33101.

Relative rate constants, k_j, for the cell-to-cell diffusion of tracer molecules of different size were determined for the cell junctions of Chironomus salivary gland. Tracers of different size and fluorescence characteristics were injected simultaneously into a cell, and the resulting fluorescence changes in this and a neighboring cell were recorded photometrically. The k_j for each tracer was determined by compartment analysis, taking into account the kinetics of intracellular tracer diffusion, loss of tracer from the cells and apparent tracer sequestration; all of these processes contributed significantly to the overall diffusion kinetics and varied considerably from tracer to tracer. Membrane depolarization was found to reduce the k_j's of both the large and small tracers equally. Furthermore, membrane potential shifts changed by the same factor both the electrical conductance of a cell junction and the k_j of a fluorescent tracer for that junction. The results indicate that junctional permeability can be varied without an accompanying change in selectivity to the permeants. This is expected if individual channels typically open and close in the all-or-none fashion.

T-AM-B4 ANALYSIS OF THE INTERDEPENDENT MODULATION OF JUNCTIONAL CONDUCTANCE BY MEMBRANE POTENTIAL, BY Ca^{2+} AND BY H^+. B. Rose, A.L. Obaid & S.J. Socolar. Dept. of Physiology and Biophysics, University of Miami School of Medicine, Miami, FL. 33101.

The cell-to-cell conductance g_j of Chironomus cell junctions is a function of the cells' membrane potentials E and of intracellular Ca^{2+} and H^+ concentrations (pCa_i, pH_i). Decrease in pCa_i or pH_i causes a parallel shift of the sigmoid g_j vs E curve to more negative E and an increase shifts the curve to more positive E, without affecting either $g_j$max or the curve's slope. In light of our model for voltage control of g_j (elsewhere in these abstracts) -- a model that analyzes g_j in terms of a population of cell-to-cell channels each with two independently controlled, bistable gates in series -- we interpret these results to indicate (1) that Ca^{2+}, H^+ and E all affect the same gates (although neither the ions nor E need act directly on them); (2) that neither Ca^{2+} nor H^+ modifies the voltage sensor that mediates gate opening/closing; and (3) that Ca^{2+} and H^+ change the standard free energy for gate opening/closing.

These studies were done on cell pairs isolated from Chironomus salivary glands. Two independent voltage clamps were used to set membrane potentials and to determine g_j.

T-AM-B5 CONTROL OF CELL-TO-CELL CHANNEL CONDUCTANCE IN CHIRONOMUS SALIVARY GLAND CELLS BY CELL MEMBRANE POTENTIALS: TWO INDEPENDENTLY REGULATED GATES IN SERIES. S.J. Socolar, B. Rose, A.L. Obaid, Dept. of Physiology & Biophysics, Univ. of Miami School of Medicine, Miami, FL 33101.

With independent control of cell membrane potentials E_1, E_2, we studied voltage control of steady state cell-to-cell conductance g_j. As $E_1=E_2=E$ is moved from, say, -80 mV to positive values, g_j traces a sigmoid curve from an upper asymptote ($g_j$max) to a lower asymptote $g_j=0$. When E_1 or E_2 is fixed and the other is varied, the results suggest that: (1) g_j is not a unique function of $E_j=E_1-E_2$; (2) the fixed potential imposes an upper limit on g_j. Hence we modelled g_j as a product of two functions, $f(E_1)f(E_2)$, where both have the same form. Our model assumes that: (1) each cell-to-cell channel has two bistable gates in series (one associated with each cell face of the junction) and conducts only when both are open; (2) at fixed E_1, E_2 the gate population on either junction face is in thermodynamic equilibrium between open and closed states; (3) the position of this equilibrium is set by the E associated with that face, as described by a conventional model; and (4) g_j is the resultant of the two independent equilibria (one on each face). The model fits well when $E_1 \approx E_2$; moreover, parameters of the model evaluated for $E_1 \approx E_2$ predict g_j -- g_j(calc.) -- accurately when $E_1 \approx -E_2$ (i.e., in presence of substantial E_j) even though E_j does not figure in the model. For other $E_1 \neq E_2$, there is a deviation g_j(calc.) - g_j(meas.) that increases as E_1+E_2 increases. This suggests that the ultimate voltage determinant of gate patency say, on side 1, is not E_1 but rather the more local perichannel membrane potential, a quantity related to E_1 but dependent also on E_2 if significant diffusion resistance occurs between the bath and the perichannel region of the intercellular gap.

T-AM-B6 GAP JUNCTIONAL CONDUCTANCE BETWEEN ISOLATED PAIRS OF VENTRICULAR MYOCYTES FROM RAT. R.L. White, A.C. Carvalho, D.C. Spray, B.A. Wittenberg, & M.V.L.Bennett. Depts. of Neuroscience & Physiology, A.Einstein Coll. of Med., Bronx, N.Y. 10461.

Electrical coupling in heart muscle was previously studied by measurements on multicellular preparations. Gap junctional conductance was difficult to quantify because of multiple current pathways and inability to record from adjacent cells. We now have recorded from pairs of isolated ventricular cells and characterized junctional and non-junctional conductances. Pairs occurred in preparations of isolated myocytes made by collagenase treatment and incubation in modified Tyrode's solution (Wittenberg & Robinson, '81, Cell Tissue Tes. 16:231). Each cell of a pair was impaled with 1 or 2 microelectrodes or recorded from with a fire-polished patch electrode forming a multi-gigohm seal, the patch membrane being broken by suction. Microelectrode recordings were made in conventional current clamp mode while patch electrode recordings were made in both current and voltage clamp modes. Cells had resting potentials from -85 to -40 mV with most negative to -60mV. Most action potentials exceeded 100 mV in amplitude and had durations of 10-50 msec. Nonjunctional conductances were 17-26 nS (40-60 MΩ). Junctional conductances were as high as 5uS (0.2MΩ). Injury decreases junctional conductance. Junctional conductance was linear for 3 sec 50 mV transjunctional voltage steps of either polarity. Linearity of this degree contrasts to several other vertebrate systems which are highly non-linear. This preparation should facilitate further study of junctional properties and pharmacology.

T-AM-B7 OSMOTIC DEFORMATION OF RED BLOOD CELL GHOSTS. Taihyun Chang, Philip B. Sharpless, Deborah A. Davenport, and Hyuk Yu. University of Wisconsin, Madison, Wisconsin 53706.

The osmotic response of red blood cell ghosts to a series of carbohydrates is studied by light scattering. The sealed and right-side out ghosts are prepared by the procedure of Steck et al, swollen in a hypotonic phosphate buffered saline solution and their size and shape determined by elastic and quasielastic light scattering. The radius thus determined in $\sim$2.3μm for bovine ghosts. Different carbohydrate are then added to the suspending medium in order to examine the osmotic responses, and the osmotic deformation of ghosts are shown to be spherically symmetric. We then rank the osmotic activity of a carbohydrate. It is found that the osmotic response of the ghosts depends on the size of sugar. Measurements with human red blood cell ghosts will be compared to those of bovine ghosts.

T-AM-B8 RED CELL FORM, VOLUME, AND DEFORMABILITY: THEORY AND EXPERIMENT. Gary V. Richieri, Steve P. Akeson, and Howard C. Mel, Department of Biophysics and Medical Physics and Donner Lab, LBL, University of California, Berkeley, CA 94720.

We have developed a simple, new approach to the determination and presentation of size, shape, and deformability information for cells, notably red blood cells. The results are obtained by combining experimental measurements from resistive pulse spectroscopy (an extension of electronic cell-sizing methodology) with theoretical calculations for model cell systems. Approximating red cell shapes by both oblate and prolate ellipsoids of revolution, values are determined for cell shape factor and volume under a variety of conditions. For red cells under normal, low stress conditions, shape factor and volume results are found to be consistent with those available from the literature. The applicability of this approach to the determination of properties of red cells under altered conditions is demonstrated in the form of results for cell volumes under conditions of altered temperature and osmotic pressure, and for cell shape (factors) under conditions of changed osmotic pressure and mechanical shear stress. Furthermore, by quantitating the change in cell shape with shear stress, a new measure of cell deformability is obtained.

T-AM-B9 EFFECT OF ERYTHROCYTE SHAPE AND VOLUME ON BLOOD FLOW IN 30μ I.D. TUBES. Colin B. McKay and Herbert J. Meiselman, Dept. of Physiology and Biophysics, Univ. of Southern California School of Medicine, Los Angeles, California 90033

Blood in narrow tubes manifests anomalous flow behaviour: both apparent viscosity and tube hematocrit decrease with decreasing tube diameter. These phenomena are known as the Fahraeus-Lindqvist and Fahraeus effects. As the tube diameter approaches that of the red blood cell (RBC), cellular properties (e.g., shape, volume, intracellular viscosity) may be expected to play a dominant role in blood flow; RBC shape and volumes are easily altered by non-isotonic buffer. Viscosity (η) and tube hematocrit (HT) were thus measured for RBC suspensions over a wide range of osmolality (169 to 730 mOsm/kg) at feed hematocrits (HF) of 40.4, 47.3 and 56.5%; 30μ I.D. tubes were employed. At all hematocrits RBC shrunk by 15% demonstrated a 16% increase in η compared to isotonic RBC. Further shrinkage to 66% of isotonic, however, resulted in HF-dependant changes: 92% increase at HF = 40.4% and 160% increase at HF = 56.5%. Conversely, RBC swollen by up to 44% showed HF-independant decrease of only 13%. Relative tube hematocrits (HT/HF) were nearly insensitive to RBC shape and volume; HT/HF changed by only 12% from the minimum value of 0.796. These small alterations in HT/HF are not sufficient to explain the viscosity results, therefore indicating that RBC shape, volume and cell-cell interactions play a major role in the microrheological behaviour of erythrocyte suspensions. (Supported by N.I.H. grants HL 15162 and 15722).

T-AM-C1 FUNCTIONAL LABELLING IN PROTEINS. S.W.Englander, J.J.Englander*, J.Ray* & A.J.Wand*. Dept of Biochemistry & Biophysics, University of Penna., Phila., PA 19104.

A functional labelling technique, based on protein H-exchange behavior, now makes it possible to selectively label and identify just those parts of a protein that participate actively in any function, and perhaps to measure the quantitative contribution of each segment in terms of free energy. When proteins engage in any interaction, a fraction of their peptide NH change their exchange rates. These sites, which presumably include functionally involved segments, can be labelled by exchange-in with isotopic H in the fast protein form; subsequent exchange-out in the slow form gets rid of label on functionally insensitive sites (exchange rate the same in both protein forms) but retains label on sensitive sites, now in their slow form. These labelled regions can then be identified.

Results from this lab and others now indicate that peptide NH tend to exchange in small sets, marking dynamical "unfolding units" of the kind pictured in the local unfolding model for H-exchange. The unfolding model connects H-exchange rate with structural free energy; therefore any change in stabilization energy produces a correlated change in H-exchange rate. To modulate functional equilibria (redox, ligand binding, E.S interaction, etc) proteins must change their structural energy with functional state. Thus H-exchange rates measured in the different protein states may indicate the energetic contribution of each involved segment to the function studied. Additionally such studies can help elucidate protein dynamical behavior and the relationship of dynamics to function. This will be illustrated with results on hemoglobin and cytochrome c.

T-AM-C2 HYDROGEN EXCHANGE RATES OF THE RAPIDLY EXCHANGING BPTI PROTONS. Erik Tuchsen and Clare Woodward, Biochemistry Department, University of Minnesota, St. Paul, MN 55108

Proteins undergo internal motions which allow replacement of buried labile ^1H atoms by ^2H from the solvent. H/D exchange rates of single protons are measured from the decrease in intensity of assigned peaks in the ^1H NMR spectrum. For rapidly exchanging protons, the exchange rates can be measured when the corresponding peaks are resolved from overlapping peaks by specific deuteration of the more slowly exchanging sites. Exchange rates have been measured for 17 rapidly exchanging protons at varying pH ($1 < pH < 8$) and temperature ($15°< T < 47°C$). For 10 of these, no rate data have been reported previously. In general these protons display simple first order catalysis by H^+ and OH^-, and the activation energy is on the order of the activation energy for exchange of peptide protons in simple model peptides. It is evident that the exchange rate at a given pH and temperature is determined not only by the dynamic accessibility and by the intrinsic exchange rate (including nearest neighbor effects), but also to a considerable extent by long range electrostatic interactions with charged side chains. Thus, the pH of minimum rate, pH_{min}, varies widely, from <1 to 3.5 for peptide protons. In addition, shifts in the pH-rate profiles of several protons are observed around pH 3-4. These apparently arise from the titration of glutamic and aspartic acid side chains.

T-AM-C3 TRYPSIN BINDING EFFECTS ON THE HYDROGEN EXCHANGE RATES OF THE BPTI ß-CORE PROTONS. Istvan Simon, Erik Tuchsen and Clare Woodward, Biochemsitry Department, University of Minnesota, St. Paul, MN 55108

The influence of trypsin binding to BPTI on the hydrogen exchange kinetics of the slowest exchanging, ß-core protons of BPTI has been measured. Exchange was allowed to take place both in free BPTI and in the complex for varying times, then the pH was rapidly dropped to pH 2 where the complex dissociates and the exchange reaction is quenched. The degree of exchange, given by the ^1H NMR intensity, as a function of time was then determined on uncomplexed BPTI, which eliminates peak broadening from the increased molecular weight of the complex. In the range 25-40°C and pH 9-10, exchange for the measureable ß-core protons is by the low activation energy mechanism. Under these conditions, exchange rates of the 8 slowest exchanging protons in free BPTI vary over three orders of magnitude, from the fastest, tyr 35, which is on the edge of the ß-core close to the surface, to the slowest which is situated in the center of the core. (This is contrast to their exchange rates by the high activation energy process at 68°, which for all 8 protons are within a factor of 2.) The three slowest exchanging protons, tyr 21, phe 22 and tyr 23, exchange too slowly under these conditions to be measured. For the other 5 protons, arg 20, gln 31, phe 33, tyr 35, and phe 45, ΔH^+_{app} is in the range 12-35 kcal/mol in both the complex and in free BPTI. All are slowed in the complex, but the degree of retardation is different for each proton. The exchange rate of gln 31, the ß-core proton most distant from the contact surface, decreases 2-3 fold, while tyr 35, the amide proton closest to the contact surface, is 10^3 times slower exchanging in the complex. Exchange rates in the complex vary over 2 orders of magnitude.

T-AM-C4 STEADY STATE AND NANOSECOND SPECTROSCOPY OF TYROSINE-TYROSINATE FLUORESCENCE IN SPINACH AND BOVINE TESTIS CALMODULIN. Shlomo Pundak and Rodney S. Roche, Biochemistry Division, Department of Chemistry, The University of Calgary, Calgary, Alberta, T2N 1N4, Canada.

A detailed study of the pH and Ca(II) dependence of the steady state fluorescence properties of bovine testis (B-CaM) and spinach (S-CaM) calmodulin reveals, under appropriate conditions of pH and pCa, a major contribution to the observed fluorescence of both proteins from singlet excited (S_1) tyrosinate (λ em = 316, 345nm; λ ex = 278-288; ionic strength = 0.015-0.020 M). In B-CaM, which has tyrosine residues at positions 99 and 138, (S_1) tyrosinate emission results from direct excitation of ground state (S_0) tyrosinate which is in ionization equilibrium with (S_0) tyrosine at pH values greater than 6.5. In contrast, the single Tyr 138 in S-CaM shows no ground state tyrosine ionization below pH 9. On the basis of the homology between the two proteins, it would appear that the more acidic ground state tyrosine in B-CaM is Tyr 99. In the case of S-CaM, nanosecond time-resolved emission spectra reveal that excited state proton transfer contributes to the observed tyrosinate emission in the pH range 5-9. Both tyrosine and tyrosinate emission show pH and Ca(II) dependent biexponential decay kinetics. In the pH range 5-9, the two lifetimes for emission from (S_1) tyrosine (λ em = 305nm) lie in the ranges 0.1-0.36 ns and 2.6-3.9 ns, and from (S_1) tyrosinate (λ em = 345nm) in the ranges 1.1-3.0 ns and 6.0-13.3 ns, respectively. The tyrosinate emission is preferentially quenched by Ca(II) in a pH dependent way with maximum quenching at pH 6.5 and 7.5. The latter "titration" suggests that the internal dynamics of the molecules are very sensitive to changes in pH and pCa in the physiological range.

T-AM-C5 OXYGEN QUENCHING AND FLUORESCENCE DEPOLARIZATION OF TYROSINE RESIDUES IN PROTEINS by Joseph R. Lakowicz and Badri P. Maliwal, University of Maryland, School of Medicine, Department of Biological Chemistry, Baltimore, Maryland 21201.

We examined the dynamics of oxygen quenching and depolarization of tyrosine fluorescence in small peptides and proteins lacking tryptophan. The oxygen quenching constants and the apparent correlation times for fluorescence depolarization were found to be sensitive to the conformational state of the proteins. For small peptides and random coil proteins the oxygen bimolecular quenching constants indicated complete accessibility of the tyrosine residues to collisions with oxygen. For folded proteins the quenching constants were about two-fold smaller, indicating only limited shielding of the tyrosine residues from oxygen by the protein matrix. We also used the steady state anisotropies, measured under conditions of oxygen quenching, to estimate the motional freedom of the tyrosine residues. For random coil proteins, such as a tyrosine copolymer and histones at low pH, the data clearly indicated that depolarization occurs due to subnanosecond segmental motions of the tyrosine residues which are independent of overall protein rotation. For some folded proteins, including bovine pancreatic trypsin inhibitor, the data are consistent with, but do not unambigiously demonstrate, motional freedom of the residues. In these cases energy transfer among tyrosine residues may also contribute to the observed depolarization. Overall, these results indicate that the rate and extent of tyrosine rotation in proteins depend upon the conformation of the protein and the specific protein under observation.

T-AM-C6 A PROTON NMR INVESTIGATION OF THE CONFORMATION AND DYNAMICS OF THE ANTIFREEZE GLYCOPROTEIN OF POLAR FISH. C. Allen Bush, B. Yamasaki, G. Matson and Robert E. Feeney. Dept. of Chemistry, Illinois Inst. of Tech., Chicago, IL. 60616 and Dept. of Food Science, Univ. of Calif., Davis, CA. 95616.

High field proton nmr spectroscopy has been used to test and refine our recent proposal, based on vacuum uv CD results, of a 3-fold left handed helical conformation for AFGP. Partial assignment of the protons of the glycotripeptide repeating unit has been made by comparison with spectra of model compounds, by selective decoupling and n.O.e. At 40°C, AFGP fraction 8 (MW = 2700 daltons) shows 2 Hz linewidths which broaden at lower temperature. Neither ^1H nor ^{13}C chemical shifts depend strongly on temperature suggesting no abrupt conformational transition. The n.O.e. between alanine α and β protons vary with temperature and with field strength from small positive enhancements at 50°C and 80 MHz to large negative effects at 3°C and 300 MHz indicating a substantial change of rotational correlation time with temperature. The higher molecular weight fractions 1-4 show negative n.O.e. at all temperatures. The CD spectra of fraction 1-4 show bands characteristic of the poly proline II structure at both 3°C and at 50°C while those bands in fraction 8 are weaker at 50° than at 3°C. We interpret the ^1H n.O.e., the ^{13}C T_1 and CD data as indicating that AFGP fraction 8 is an extended rigid rod in the poly proline II conformation at low temperature which becomes a flexible coil at high temperature while fraction 1-4 is a flexible rod whose persistence length is approximately the size of a fraction 8 molecule.

T-AM-C7 INTERNAL DYNAMICS OF HEMOGLOBIN.--J. M. Friedman and T. W. Scott, Bell Laboratories, Murray Hill, New Jersey 07974

Using time resolved Raman spectroscopy, we have followed the relaxation dynamics of the Fe-proximal histidine linkage in photodissociated carboxy hemoglobins. We observe that with respect to this structural parameter, the protein retains memory of both the quaternary state and the state ligation for lengths of time that strongly depend upon factors that are known to destabilize the structure of the ligand bound hemoglobin. At pH7 and lower the relaxation of the histidine associated tertiary structure is apparent within 10's of ns subsequent to photolysis. Since geminate recombination is known to occur on this time scale and since the Fe-His linkage has been implicated[1] in the mechanism by which the barrier height controlling ligand binding is protein modulated, these results raise the possibility of kinetic cooperativity in hemoglobin. This idea is further supported by our transient Raman studies which reveal that competition between the time scales for tertiary structure relaxation and for ligand rebinding subsequent to spontaneous dissociation is responsible for temperature dependent changes in the oxygen binding properties of HbA.

1. J. M. Friedman, R. A. Stepnoski and R. W. Noble, FEBS Letters 146, 278 (1982).

T-AM-C8 MOLECULAR DYNAMICS AND LIGAND BINDING IN HEME PROTEINS. William Bialek and Robert F. Goldstein, Department of Biophysics and Medical Physics, University of California, Berkeley, California 94720

The dynamics of heme proteins need not be interpreted in terms of "conformational substates"(1) among which the molecule fluctuates. We show that the available data are in fact consistent with nearly harmonic vibrations of the protein about a single equilibrium conformation. Temperature-dependent Debye-Waller factors in Mossbauer and crystallographic experiments may be interpreted in terms of the spectrum of low-frequency vibrational modes of the molecule, and anomalous features of the infrared and Raman spectra are accounted for by weak anharmonic interactions. We apply radiationless transition theory(2) to analyze the ligand binding reaction, and show that the cross-over from molecular tunneling to Arrhenius behavior is quantitatively related to the low-frequency vibrational spectrum of the protein. The non-exponential time course of the reaction(3) can be accounted for in terms of inhomogeneous broadening of these vibrational lines.

1. Frauenfelder, H., G.A. Petsko, & D. Tsernoglou, Nature 280:588 (1979).
2. cf. Jortner, J. & J. Ulstrup, J. Am. Chem. Soc. 101:3744 (1979).
3. Austin, R.H., et al., Biochemistry 14:5355 (1975).

Supported by the NSF (PCM 78-22245 and pre-doctoral fellowship to W.B.) and the U.S.D.O.E. through the Lawrence Berkeley Laboratory.

T-AM-C9 **Structural Dynamics in Hemoglobin and Myoglobin Probed by Resonance Raman Scattering at Cryogenic Temperatures** D. L. Rousseau *Bell Laboratories, Murray Hill, New Jersey 07974, and* M. R. Ondrias *University of New Mexico, Albuquerque, New Mexico 87131*

The importance of molecular dynamics in the functional properties of hemoglobin and myoglobin is widely recognized. Dynamics are evident locally in changes at the heme on the binding and release of oxygen and globally both in movements of amino acid residues allowing passage of small molecules to the binding sites and in quaternary structural rearrangements of the large protein subunits altering the ligand binding affinity. These changes are very complex and difficult to study because under physiological conditions they occur on time scales ranging from subpicoseconds to several microseconds. However, by freezing hemoglobin or myoglobin at cryogenic temperatures protein conformations are stabilized and intermediates in the reaction pathway may be isolated for long periods of time. Thus, structural changes in the time domaine which occur under physiological conditions are transcribed to changes in the temperature domaine under cryogenic conditions.

We have examined the resonance Raman spectrum of deoxyhemoglobins and deoxymyoglobins prepared by freezing the carbonmonoxy forms of these proteins at cryogenic temperatures and photodissociating the CO with a laser beam. We find substantial differences in the heme Raman spectrum when comparing these intermediate forms to the respective equilibrium deoxy preparations under identical conditions. Furthermore, there are qualitative differences between the behavior of hemoglobin and myoglobin. We conclude from these data that ligand binding necessitates larger structural rearrangements in the heme pocket of hemoglobin than it does in the heme pocket of myoglobin. These differences in the structural dynamics may be related to the functional differences in the ligand binding affinities of these two proteins.

T-AM-C10 LTRAVIOLET RESONANCE RAMAN STUDIES OF PROTEIN COMPONENTS. Bruce Hudson, Larry Ziegler, Duane Flamig and Daniel Gerrity, Department of Chemistry and Institute of Molecular Biology, University of Oregon, Eugene, OR 97403.

Recent advances in laser technology permit the generation of ultraviolet radiation suitable for Raman studies with wavelengths as short as 188 nm. Raman studies of protein components using 200 to 270 nm excitation have revealed several new resonance enhancement, isotopic substitution and hydrogen bonding effects. The model peptide N-methylacetamide shows a strong amide II band when excited at 213 nm. This band is not observed in visible excitation Raman spectra. Deuterium substitution of the amide proton results in a dramatic change in the amide II to amide III intensity ratio such that amide II' is by far the strongest band. The implication of this observation in terms of the normal modes and geometry change upon electronic excitation will be discussed. Another interesting observation is that the amide I C=O stretch band of N-methylacetamide is very broad in dilute aqueous solutions but sharp in acetonitrile. Results for other simple peptides will also be discussed. Proline has a very characteristic spectrum similar to that of deuterated N-methylacetamide. Several common residue side chains give strong, characteristic spectra with ultraviolet excitation. Fluorescence is not a problem because the Raman emission is at a much shorter wavelength than the fluorescence interference. The spectra of tryptophan, tyrosine, phenylalanine, histidine-H^+, histidine-D^+ and arginine will be presented. The state of protonation and isotopic substitution of histidine produces large spectral changes and the state of ionization of tyrosine is easily determined. Recent results for globular proteins will also be presented. Those containing tryptophan are dominated by the strong bands of this residue.

T-AM-C11 TERTIARY STRUCTURE OF LENS PROTEIN: CHANGES DURING CATRACTOGENESIS. B. Chakrabarti, J.N. Liang and U.P. Andley. Eye Research Institute, Boston, MA 02114.

Studies to date have emphasized that the molecular basis of lenticular transparency is intimately related to the molecular shape and arrangement of the lens proteins, which in turn depend on the local environment of different amino acids and on the reactive groups and their interaction properties. Results of our recent studies have elucidated the conformational aspects of lens crystallins and the accessibility and arrangements of different amino acids and groups that are known to be vulnerable to changes during cataractogenesis (Biochemistry 21:1847, 1982; 21:1853, 1982). As a model for senile and diabetic cataract, we have studied bovine lenses of different age groups and the effect of sugar molecules and UV light on the crystallins. Spectroscopic studies (CD and fluorescence) of α-crystallin indicate that distinct differences exist in the tertiary structure of the protein of young and old bovine lenses and also of the nucleus and cortex of the lens. In accordance with our previous report we find that α-crystallin is more vulnerable to photooxidation (as tryptophan residues of this protein are more exposed) than the other two crystallins. Changes in the tertiary structure, as manifested in the near-UV CD, have also been noted when crystallins are incubated with sugar molecules or upon irradiation with UV light; structural changes are followed by aggregation of the proteins, presumably a common phenomenon in the cataractous lens. Results of our CD, fluorescence, and photochemical studies of lens crystallins will be reviewed and discussed in light of tertiary structure and its possible changes during cataractogenesis.

T-AM-D1 INITIAL CONDITIONS AND SODIUM AND GATING CURRENT TIME SHIFTS. Robert E. Taylor, and Francisco Bezanilla, NINCDS, NIH, Bethesda, MD 20205; Dept. of Physiology, UCLA, Los Angeles, CA 90024.

Giant axons of the squid Loligo pealei were cleaned, perfused and voltage clamped. Ionic and gating currents were recorded using the P/4 procedure with negative subtracting holding potentials. Gating currents, as well as sodium currents, were delayed, with little change in shape, by a hyperpolarizing prepulse. The delay seems to be saturated, at about 45 μsec, for prepulses to -140 mV and, at 8°C, develop with time constants of between 60 and 180 μsec. At lower temeratures the shifts are much larger. The time delay of the sodium current, as the magnitude of the hyperpolarizing prepulse is increased, is correlated with the extra charge which moves during the gating current. From these results we conclude that the gating current, including the charge moving for potentials more negative the -70 mV, is indeed closely associated with the process of sodium channel activation and they provide information concerning the kinetics of the early steps which are hidden in ionic current measurements. The gating and sodium current time shifts and the correlation between charge movement and time shifts are approximately duplicated by a simple sequential model with six states. The experiments were done at the Marine Biological Laboratory, Woods Hole, MA and were supported by UPHS grant GM 30376.

T-AM-D2 ACTIVATION GATING OF NERVE SODIUM CHANNELS: SIMULATIONS. C.M. Armstrong and D.R. Matteson. Department of Physiology, University of Pennsylvania, Philadelphia, Pa.
We have simulated conductance, gating current, and single channel behavior for a four state model of Na channel activation

$$\text{closed } 3 \underset{b_3}{\overset{a_3}{\rightleftharpoons}} \text{closed } 2 \underset{b_2}{\overset{a_2}{\rightleftharpoons}} \text{closed } 1 \underset{b_1}{\overset{a_1}{\rightleftharpoons}} \text{open}$$

assuming equal gating charge movement for each step. Three closed and one open state are the minimum requirement for reproducing the sigmoid rise and exponential deactivation of Na channels in squid nerve. Conductance time course is little affected when the rate constants are varied from 9:6:3 (a_3:a_2:a_1) to 5:5:5 to 3:6:9. The same alterations cause a qualitative change in the predicted gating current, from exponential to initially flat to initially rising (simulation of a large depolarization). The equations for the histograms of a single channel are the same as for macroscopic currents, if rate constants and initial conditions are properly chosen. That is, macroscopic current of the sequence above duplicates the open time histogram when $a_1 = 0$, all channels initially open; the closed time histogram when $b_1 = 0$, all initially in closed 1; and latency to first opening when $b_1 = 0$, all initially in closed 3. Varying the transition rates among closed states most strongly affects gating current time course and the closed time histogram.

T-AM-D3 **VOLTAGE CLAMP EXPERIMENTS ON GH3 CELLS**
D. R. Matteson and C. M. Armstrong, Department of Physiology, University of Pennsylvania, Phialdelphia, PA.

The whole cell variant of patch clamp technique was used to study GH3 cells (see Ohmori and Hagiwara, Biophys. J. *37*: 20a). On breaking the cell, the capacitance increased by 10-30 pf, or roughly 1-2 $\mu f/cm^2$ of cell surface. The ionic current pattern was extremely stereotyped. With 130 NaCl 10 $CaCl_2$ // 140 KCl EGTA outside//inside, there was a transient inward current and a sustained outward current. The outward current was blocked by internal Ba^{++} and was very small or absent with isotonic internal Cs^+. In 130 NaCl 10 $CaCl_2$ // 140 CsCl EGTA, the inward current had a peak amplitude of roughly 0.2 to 1.5 nA and was clearly resolvable into a fast and a slow component. The fast current was absent when Tris was substituted for Na externally. In 130 NaCl 10 $CaCl_2$ // 140 NaCl EGTA, the fast current was outward and the slow current inward at +10 or +20 mV. After an activating pulse to +20 with return to —70 mV, there was a rapidly decaying tail if the pulse was about a millisecond or less, and a fast and a slow tail for pulses from roughly one to two milliseconds, and, predominantly, a slow tail for longer pulses. The slow tail was largely inactivated after a pulse of 100 ms.

T-AM-D4 MB1: EFFECTS OF METHYLENE BLUE ON SODIUM IONIC CURRENT AND GATING CURRENT.
J.G. Starkus, M.D. Rayner, S.T. Heggeness. University of Hawaii, Dept. of Physiology, Honolulu, HI

The interactions of internal MB with sodium channel were studied both in nonpronased and pronased crayfish axons. In normal axon with intact h, MB exhibited a voltage and time dependent block but no frequency dependent block at 1 Hz. The kinetics of MB block were studied in more detail from pronased axons with the data being expressed as % block calculated from 100 $(I_C-I_{MB})/(I_C-I_gON)$. This analysis exposed the intrinsic kinetics of MB block. Results indicate two types of block--tonic and time dependent. Tonic block appears concentration dependent but not voltage dependent suggesting that the site is superficial to the transmembrane voltage field. Time dependent block appears to be both concentration and voltage dependent suggesting a site deep within the inner regions of the pore. Time dependent block exhibits a single exponential with time constants of 1190±72 μs and 270±4 μs for 50 μM and 500 μM at 0 mV (60°C).

MB tail currents are slower than normal tail currents and exhibit a pronounced hook. Kinetics of MB tail currents are pronase sensitive, being faster after h gate removal. Dissociation of MB seems to be slowed by the presence of h gate.

ON and OFF gating currents are suppressed when internal MB acts synergistically with external TTX. The magnitude of this suppression is hold potential dependent, increasing with lower hold potentials and decreasing with higher hold potentials. The kinetics of the ON gating current are not affected by MB but the kinetics for OFF gating currents are retarded. Results indicate that MB can reach the time-dependent site only after m gates open and prevents m-gate closure when bound at this site. Thus MB interacts with both m and h-gates in binding to the time-dependent receptor.

T-AM-D5 MB2: ANALYSIS OF TIME-DEPENDENT BLOCK OF SODIUM AND GATING CURRENTS BY METHYLENE BLUE IN PRONASE-TREATED CRAYFISH GIANT AXONS.
M.D. Rayner, J.G. Starkus, and S.T. Heggeness, University of Hawaii, Dept. of Physiology, Honolulu, HI 96822.

Internal perfusion of pronase-treated axons with methylene blue (MB) produces a time-dependent "open pore" block of sodium currents which may be interpreted as a pseudo-first order reaction in which $[MB]_i$ remains constant. Eliminating control sodium kinetics using point-by-point comparison between MB-treated and control sodium currents, both tau_{MB} and equilibrium block (B) can be directly evaluated from signal-averaged traces. The forward reaction rate ($K_{1,2}$) can then be calculated as B/tau_{MB} while the reverse rate is $(1-B)/tau_{MB}$. Consistent with this model, only $K_{1,2}$ is affected by $[MB]_i$ although both $K_{1,2}$ and $K_{2,1}$ are voltage-dependent with a slope indicating a binding site deep within the sodium pore. K_D at 0mV is 40 μM.

Tail currents in presence of MB are quantitatively consistent with this model if it is presumed that bound MB prevents "M"-gating closure. Observed tail currents can be predicted from the MB dissociation rate and control "M"-kinetics in a three-state sequential reaction scheme.

Slight suppression of gating current (I_g) by MB is predicted by this model, since some binding of MB occurs at hold potentials less negative than -100 mV. Q-V_m plots demonstrate that the additional marked suppression of I_g by MB in presence of TTX is relieved at very negative hold potentials. The slope of this relationship suggests an apparent shift of the MB binding site within the transmembrane field following exposure to TTX. (Supported in part by NIH Grant No. GM29263-03 and U.H. Research and Training Grant.)

T-AM-D6 MOLECULAR STRUCTURE OF THE VOLTAGE-DEPENDENT Na^+ CHANNEL,
Kimon J. Angelides and Thomas J. Nutter, Departments of Biochemistry and Molecular Biology and Neuroscience, University of Florida, College of Medicine, Gainesville, Florida 32610.

In excitable cells the action potential is produced by sequential time and voltage-dependent changes in the membrane permeability to Na^+ and K^+ ions controlled by intrinsic membrane proteins.

Tetrodotoxin (TTX), batrachotoxin (BTX), and the scorpion toxins (Leiurus q. and Centruroides s.) have been used with considerable success to probe specific components of the sodium conductance. We have prepared and purified by novel chemical techniques a number of biologically active fluorescent derivatives of TTX, ScTX and BTX which have been characterized electrophysiologically, by equilibrium binding, and spectroscopically. The activities of these toxins are only 1.5-8 times lower than the native toxins. These site specific probes have been used to map the molecular structure of the axonal and synaptosomal Na^+ channel by fluorescence singlet-singlet energy transfer. Efficiencies were measured both by donor quenching and acceptor sensitized emission. To evaluate distances between multiple donor-acceptor pairs the positions of the chromophores were exchanged. The following distances between neurotoxin receptor sites on the channel have been determined: TTX to Centruroides s., 33 Å; BTX to Leiurus q., 37 Å; Centruroides s. to Leiurus q., 22 Å; TTX to Leiurus q., 35 Å. In the presence of the allosteric activator BTX, the TTX to Leiurus distance changes to 42 Å. From these data a high resolution molecular structure of the Na^+ channel has been formulated. Preliminary data on the intramembrane location of these sites will be presented. These fluorescent neurotoxins have also been used to microscopically visualize sodium channels in excitable cells.

T-AM-D7 IRREVERSIBLE MODIFICATION OF SODIUM CHANNEL INACTIVATION BY CHLORAMINE-T.
Ging Kuo Wang and Gary Strichartz, Anaesthesia Research Laboratories, Harvard Medical School, 75 Francis St., Boston, MA 02115

Chloramine-T is a mild oxidant which can specifically modify the methionine and cysteine residues of proteins (Shechter, et al., 1975. Biochemistry 14:4497). When single amphibian myelinated nerve fibers were treated externally with chloramine-T, at concentrations from 0.2 - 0.6 mM, the action potentials were prolonged irreversibly, from a normal duration of 5-8 msec to durations as long as 4 sec (with CsCl intracellularly, at 8°C). Under voltage clamp conditions, two distinct modifications were resolved. Firstly, a non-inactivating component of sodium conductance appeared, resulting in a maintained sodium current which declined with a time constant too slow to be measured accurately ($t_{\frac{1}{2}}$ >> 2 sec) during a prolonged depolarization. Secondly, the steady-state sodium inactivation (h_∞) of the remaining current was shifted by 20 mV to the depolarized direction, reducing the extent of resting inactivation. The shift in h_∞ occurred much more rapidly than the development of non-inactivating currents. Thus, there are at least two separate sites modified by chloramine-T which are involved in the inactivation processes. Chloramine-T has no apparent effect on the sodium channel activation, judging from the measurement of repolarization tail currents, activation time course and voltage-dependence of peak currents, and the effect of elevated Ca^{2+} on voltage-dependence of peak currents.

Unlike purified Leiurus scorpion toxin, chloramine-T treatment does not potentiate veratridine's ability to depolarize the resting membrane of the sciatic nerve. We conclude that slowing or removing of sodium channel inactivation alone is not sufficient for the potentiation of the activator's effect. Supported by Grants from USPHS (NS-18467 and the Multiple Sclerosis Fdn

T-AM-D8 COMBINED INFLUENCE OF GUANIDINE DERIVATIVES AND TETRODOTOXIN ON Na CHANNEL GATING AND IONIC CURRENTS IN SQUID AXON MEMBRANES. Jay Z. Yeh, George R. Ehring and Stephen Vogel, Dept. of Pharmacology, Northwestern University Medical School, Chicago, IL 60611.

Octylguanidine (C_8-G) and tetrodotoxin (TTX) block the Na ionic current (I_{Na}) from an internal and external membrane site, respectively, without affecting the ON gating current (I_g). However, the combined application of C_8-G internally and TTX externally does suppress the ON I_g. In this study, we tested whether C_8-G and TTX would also interact in suppressing I_{Na}. First, the potency of TTX in blocking I_{Na} was determined with and without C_8-G. The dissociation constants in the absence and presence of 30μM C_8-G were 4.20 ± 0.98 (SD) and 4.76 ± 0.72 nM, and were not significantly different, as predicted from a model in which C_8-G and TTX bind independently to two distinct sites. Secondly, the effect of C_8-G on the ON I_g was compared in media containing 10% or 0% Na. C_8-G did not suppress the ON I_g regardless of the presence of Na ions (unless TTX was present externally). Hence, the interaction between TTX and C_8-G did not arise from an indirect action of TTX to prevent external Na ions from entering the channel and displacing C_8-G. Thirdly, propylguanidine (C_3-G) and octylbisguanidine (G-C_8-G), were used to study the hydrophobic contribution to the interaction. Like C_8-G, C_3-G (6 mM) and G-C_8-G (0.1 -1.0 mM) suppressed I_{Na} without affecting the ON I_g. However, unlike C_8-G, they did not reduce the ON I_g in the presence of TTX. These results suggest that a hydrophobic component of the internal blockers is essential for the observed interaction between C_8-G and TTX on the ON I_g.

T-AM-D9 VOLTAGE-CLAMP CURRENTS, NOISE AND ADMITTANCE INDICATE SIMULTANEOUS NH_4^+ MOVEMENTS THROUGH THE FAST AND SLOW CHANNELS OF SQUID AXON. H.M. Fishman, H.R. Leuchtag and D. Poussart. Univ. of Texas Med. Branch, Galveston; Texas Southern Univ., Houston; Université Laval, Quebec.

Squid axons internally perfused with a buffered Cs solution and bathed externally with NH_4-ASW (Na replaced by NH_4) were voltage clamped by an axial electrode technique. The step clamp inward current was composed of two distinct time courses: A transient, similar to that observed in Na-ASW but with only ~40% of the amplitude, and a steady-state component four or more times larger than in Na. The transient current was eliminated with TTX (1μM) added to the NH_4-ASW, but the maximum steady-state current was reduced by only ~15%. Complex admittance and current noise measurements made in the steady state required a two-time-constant model for adequate fits. When compared to corresponding data at the same potentials and in the same axon in Na-ASW, the time constants indicate an interaction between normal fast and slow channel kinetics. However, at potentials for which the TTX-sensitive steady-state inward current is small relative to the other component, two time constants are still required. These data suggest that NH_4^+ moves inward through both the fast ("Na") and slow ("K") channels simultaneously. Preliminary analysis of both noise and admittance data indicates that the kinetics of NH_4^+ through the slow channel are at least second order compared to first order for K, whereas the kinetics of NH_4 through the fast channel appear to be similar to Na kinetics.

Supported by NIH grant NS11764 and CRC grant A-5274.

T-AM-D10 SCORPION TOXIN SHIFTS SLOW I_{Na} INACTIVATION IN NEUROBLASTOMA CELLS
I.Spector and F.J.Sigworth,Dept.Anat.Sci.,SUNY ,Stony Brook,N.Y. and Max-Planck-Inst. Biophys. Chemie, Göttingen, F.R.G.

Sodium currents in N1E-115 cells show a prominent slow inactivation process (Huang et al.,PNAS 79,2082,1982) that is strongly shifted in the presence of 10-40nM scorpion toxin (Leiurus). Using the tight-seal, whole-cell clamp technique we observed a shift of the midpoint of the slow inactivation curve from near -60mV to near -30mV. At the same time, inactivation kinetics were slowed and a steady current was activated at large depolarizations, as seen in squid axons (Gillespie and Meves, J.Physiol. 308,479,1980). Single-channel recordings showed essentially no change in conductance but an increase in channel open time. Single-channel currents were -1,7pA at 20°C, essentially independent of voltage over the range -40 to -80mV. Spontaneous channel openings that occurred in the presence of ScTX during prolonged depolarizations showed the same lifetime and conductance as those elicited by pulses to the same potential, implying that the open states are the same.
A shift in the voltage dependence of slow inactivation may explain the action of ScTX on "nonexcitable" cells having low resting potentials. The shift is also consistent with a voltage-dependence of toxin binding (Catterall, J.Biol.Chem. 252,8660,1977).

T-AM-D11 **SINGLE CHANNEL CURRENTS FROM FROG LENS EPITHELIAL CELLS.**
J.L. Rae and R.A. Levis, Depts. of Physiology and Ophthalmology, Rush Medical College, Chicago, IL 60612.

Single channel recordings obtained by the patch clamp technique are now common from a wide variety of tissues. However to date there have been few reports of single channel currents obtained from epithelia. Using improved headstage electronics and alumina silicate glass electrodes, we have been successful in patch clamping the epithelium of the lens of the frog eye. This preparation allows recording from adult epithelial cells without prior enzymatic treatment. Seals from 50-900 GΩ have been obtained with regularity and at least four channel types with conductances of 120 pS, 50pS, 30pS, and 10pS and linear IV relationships have been seen. Either 50pS or 30pS channels occur in most patches, with each patch usually containing 3-5 channels of a given type. The 50pS channel reverses at the resting potential for on-cell patches with Ringer-filled electrodes and at zero mV in pulled off patches with a large Cl^- gradient across the patch, leading to its tentative identification as a K^+ channel. The 30pS channel has a 1.5-2pA inward current with a Ringer electrode on-cell patch and no applied potential. The current reverses about 60 mv positive to the resting potential. This is tentatively identified as a non-selective cation channel. Both of these channels show bursting behavior with many openings per burst but the 30 pS channel flickers at a particularly high rate. **(Supported by grants from NIH EY03282, Louise B. Norton Trust and Regenstein Foundation)**

T-AM-E1 THE ROLE OF LC2 IN SKELETAL ACTOMYOSIN ATPase AND IN MINIFILAMENT FORMATION. S.S. Margossian, H.S. Slayter & A. Bhan*. Depts. of Biochem. and Med., Albert Einstein College Med., Montefiore Med. Center, Bronx, N.Y. and Sidney Farber Cancer Institute, Boston, MA.

Myopathic hamster protease (Bhan, et al., J.Biol. Chem. 256, 7741 (1981)) was used to remove LC2 from rabbit muscle myosin. In contrast to cardiac myosin, the protease cleaved the heavy chains in addition to LC2 in skeletal myosin. However, monodisperse LC2-deficient myosin was obtained by chromatographing the digestion mixture on a DEAE Sephadex-A50 column. The supernatant from the digest contained S1 which was subsequently resolved into S1·A1 and S1·A2 isoenzymes. The Ca^{2+}- and EDTA-activated ATPases of LC2-deficient myosin were similar to those of the control, indicating no irreversible damage to the heavy chains. Double reciprocal plots of actin-activated ATPases were biphasic: at either high or low actin concentrations, there was a 50% reduction in the actin-activated ATPase of LC2-deficient myosin. Moreover, when purified LC2 was recombined with LC2-deficient myosin, the actin-activated ATPase was completely restored to control levels. Electron microscopy of shadow-cast molecules of control and LC2-deficient myosin revealed that in the control, the S1 heads had a "pear"-shaped appearance whereas in LC2-deficient myosin, the S1 heads appeared rounder and with less mass in the "neck" region (Flicker, et al., Biophys. J. 33, 279a (1981)) suggesting that LC2 lies at least partly in the S1/S2 junction. No obvious differences in the morphology of control, LC2-deficient and LC2-recombined minifilaments (Reisler, et al., J. Mol. Biol. 143, 129 (1980)) could be detected. These results indicate that LC2 is not directly involved in the assembly of myosin into minifilaments.

(Supported by NIH Grants HL26529 to SSM and GM14237 to HSS).

T-AM-E2 LIGHT-CHAIN MOVEMENT AND REGULATION IN SCALLOP MYOSIN. A. G. Szent-Györgyi, T. Wallimann and P. M. D. Hardwicke, Department of Biology, Brandeis University, Waltham, Massachusetts 02254 and ETH Eidgenossische Hochschule, Institut fur Zellbiologie, Zurich, Switzerland.

Relative movement between scallop myosin regulatory light-chains (R-LC) and essential light-chains (SH-LC) was estimated at rest, in rigor and during activity with the aid of heterobifunctional photosensitive cross-linkers attached to the R-LCs. The cross-linkers used had a length of less than 9A. 4-7 lysine residues of scallop R-LC (in unknown positions) were substituted with n-hydroxy-succinimidyl-4-azidobenzoate, the single cysteine residues of Mercenaria R-LC (position ca 50), of gizzard R-LC (position 108), and rabbit R-LC (positions 129 and 157) were substituted with p-azidophenacylbromide or benzophenone-4-maleimide. Cross-linking of R-LCs with SH-LCs and calcium regulation of the ATPase activity depended on the position of the cross-linker on the R-LC and on the conditions of photolysis. The N-terminal part of the R-LC cross-linked only if photolyzed in rigor solution (no ATP) and the cross-linking of this region resulted in a decrease of calcium sensitivity (Mercenaria R-LC). The C-terminal part of the R-LC cross-linked extensively with SH-LC both in rigor and relaxing (ATP, no calcium) solutions without an effect on calcium regulation (gizzard and rabbit R-LCs). Scallop myosin filaments hybridized with Mercenaria R-LC behaved as myofibrils and also cross-linked in activating solution (ATP and calcium). The results indicate that the light-chains move from a distance less to one greater than about 9A; that the movement is restricted for the most part to the N-terminal region of the R-LC; that it occurs on myosin before combination with actin; and that it is associated with the "on" and "off" states of myosin. (Supported by NIH AM-15963 and MDA grants).

T-AM-E3 TROPOMYOSIN CAN BE CROSS-LINKED TO MYOSIN SUBFRAGMENT-1 IN RECONSTITUTED SKELETAL MUSCLE THIN FILAMENTS. Terence Tao and Mark Lamkin. Dept. of Muscle Research, Boston Biomedical Research Institute, Boston, MA 02114.

We have used the technique of photochemical cross-linking to study the proximity between Tm[1] and S1 in reconstituted rabbit skeletal muscle thin filaments. Lysine residues of Tm were labeled with the bifunctional photo-affinity cross-linker Suc-ANPH. After irradiating the S1.ANPH-Tm.F-actin rigor complex for 5 minutes, the appearance of a band of lower mobility than that of S1 heavy chain was detected by gradient polyacrylamide gel electrophoresis. If irradiation was carried in the presence of excess sodium pyrophosphate (which is known to dissociate S1 from F-actin filaments), no low mobility band was formed. By means of differential isotope labeling, this low mobility band was identified as a cross-linking product between one ANPH-Tm chain, and one S1 heavy chain. These findings suggest that Tm is located relatively near S1 in the thin filament, as would be required in the steric blocking model for thin filament regulation. It is not clear, however, whether Tm and S1 are actually in contact with other as suggested by recent structural studies (Taylor & Amos, J. Mol. Biol. 147, 297(1981)), since the cross-linker extends ~20 A^{o} when fully stretched, with a most probable end-to-end distance of ~14 A^{o}_{1}. Similar work using shorter cross-linkers is in progress to clarify this point.

([1]Abbreviations used: Tm, tropomyosin; S1, chymotryptic myosin subfragment-1; Suc-ANPH, N-succinimidyl-6(4'-azido-2'-nitrophenyl amino) hexanoate; ANPH-Tm, Suc-ANPH labeled Tm).

(Supported by N.I.H. AM21673).

T-AM-E4 A MONOCLONAL ANTIBODY SPECIFIC FOR THE S1 HEAVY CHAIN OF MYOSIN. P. Wachsberger, and F. A. Pepe. Dept. of Anatomy, School of Medicine, U. of Penna., Philadelphia, PA 19104.

Using tryptic digests of S1 (Mornet, D. et al, Biochem. Biophys. Res. Commun. 89, 925, 1979) we have shown that a monoclonal antibody raised to chicken pectoralis myosin binds to the 27K and 20K fragments of the S1 heavy chain. The antigenic determinant recognized by the antibody is not related to the ATPase sites of myosin as the antibody does not inhibit actin-activated Mg-ATPase or EDTA-activated ATPase. The actin binding sites of myosin are not involved in the antigenic determinant, as antibody binding to native myosin filaments in myofibrils is not altered by the attachment of myosin cross-bridges to actin. With native thick filaments, in the absence of ATP the antigenic determinant is available for antibody binding in a narrow band on each side of the bare zone region and in a narrow band at each end of the filament near the A-I junction, regardless of the sarcomere length of the myofibril. In the presence of ATP, the antigenic determinant is available for antibody binding along the entire length of the myosin filament, except for the bare zone region in the middle of the filament. These findings suggest that a) differences in molecular packing in different parts of the filament may be responsible for differences in antibody binding, and b) ATP binding to S1 may alter the antibody binding as a result of change in packing and/or conformational change in the S1.

T-AM-E5 MYOSIN TOPOGRAPHY BY IMMUNO-ELECTRON MICROSCOPY USING MONOCLONAL ANTIBODIES. Donald A. Winkelmann and Susan Lowey. Rosenstiel Center, Brandeis University, Waltham, MA 02254.

Monoclonal antibodies which react with antigenic determinants in the head and rod regions of myosin and the $LC2_f$ myosin light chain have been prepared by the lymphocyte hybridoma technique after immunization of mice with chicken pectoralis muscle myosin. The specificity of the antibody secreted by cloned cell lines was characterized by radioimmunoassay, electrophoresis/immunoblots ("Westerns"), immunofluorescence and immuno-electron microscopy. These antibodies are selective for fast skeletal myosin isozymes, since they show few cross-reactions with myosins from slow skeletal, cardiac and smooth muscles. Several antigenic determinants have been localized on myosin by electron microscopy of platinum replicas prepared by rotary shadowing of antibody-myosin complexes. An antibody which reacts specifically with an amino-terminal 27,000 dalton fragment of myosin S1 maps to a single site on the myosin head. Anti-S1(12C5.3) IgG and Fab were observed binding approximately 145Å from the head-rod junction at the point where the myosin head appears thickest. An antigenic determinant on the $LC2_f$ light chain mapped to the "neck" region near the junction of the head to the rod. This location is very similar to that found for the regulatory and essential light chains on scallop myosin by Flicker et al. (1981) Biophys. J. 33, 279a. An anti-LMM (5C3.2) antibody which reacts with adult fast but not embryonic myosin was found to bind to the carboxy-terminal end of the myosin rod. These data provide direct evidence for the location of a portion of the 27K peptide in the myosin head, the position of the $LC2_f$ light chain and the distribution of isozyme specific antigenic determinants on myosin. (Supported by grants from NIH, NSF and the Muscular Dystrophy Association.)

T-AM-E6 LOCALIZATION OF A REGION RESPONSIBLE FOR THE LOW IONIC STRENGTH INSOLUBILITY OF MYOSIN. R. C. Lu, L. Nyitray, M. Balint & J. Gergely. Dept. of Muscle Res., Boston Biomed. Res. Inst., Boston, MA 02114 & Dept. of Biochem., Eotvos Lorand Univ., Budapest, Hungary

Light meromyosin (LMM) preparations are often heterogenous, containing several polypeptide chains, LMM-A, LMM-B, and LMM-C differing slightly in M_r. Limited tryptic digestion of LMM produces well defined fragments (Balint et al, JMB 37, 317, 1968). Fragments, LF-1, LMM-D, LF-2, and LF-3 with chain of mass 63 kDa, 56 kDa, 47 kDa and 30 kDa, respectively, have been isolated and characterized. Our results show that LMM-A, LMM-B, LMM-C and LF-1 have the same N-terminal sequence: GKQAFTQQIEELKDQ.., while that of LMM-D, LF-2 and LF-3 is: NFDKILAEGKHKYEE... Based on these results, the time course of the changes in the SDS-gel pattern of the digests, and their chain masses estimated from SDS gel electrophoresis, the following scheme can be deduced:

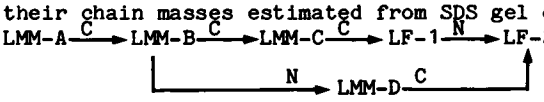

C and N over the arrows indicate removal of residues from C- and N-term.,respectively.

The positions of the peptides along the rod portion have been established by comparison with the primary structure of nematode myosin (McLachlan and Karn, Nature 299, 226, 1982). LMM and fragment LMM-D are insoluble, whereas LF-1, LF-2, and LF-3 are soluble at low ionic strength. The solubility properties in conjunction with their locations along the myosin heavy chain have enabled us to reach the conclusion that a relatively small stretch of peptide (chain mass= 5 kDa) located near the C-terminus of myosin heavy chain is responsible for the insolubility of LMM at low ionic strength. (Supprted by NIH, NSF, AHA and MDA).

T-AM-E7 IDENTIFICATION OF SITES ALONG MYOSIN ROD SUSCEPTIBLE TO PROTEOLYTIC ENZYMES. Renne Chen Lu & Anna Wong, Dept. of Muscle Res., Boston Biomed. Res. Inst., & Dept. of Neurology, Harvard Medical School, Boston, MA 02114

The myosin molecule contains two main protease sensitive regions: one is located at the head/rod (neck) joint and the other within the rod. An earlier study has shown that the N-termini of tryptic and chymotryptic subfragment-2 (S-2) are only two residues apart (Lu, PNAS 77, 2010, 1980) and the presumptive hinge of high proteolytic susceptibility is in the C-terminal part of long S-2, which is adjacent to light meromyosin (LMM). To further understand the flexible nature of the hinge region, we investigated the susceptible sites at the S-2/LMM joint. LMM produced by tryptic digestion (LMM_T) has the following N-terminal sequence: GKQAFTQQIEELKDQ.... LMM made by chymotryptic cleavage (LMM_C) is smaller than LMM_T and less homogenous at the N-terminus. The major species of LMM_C begins: ETDAIERTEELEEAK.... Using the primary structure of the rod portion of nematode myosin (McLachlan & Karn, Nature 299, 226, 1982) as reference, and based on the homology between rabbit skeletal and nematode myosin our results show that LMM_T and LMM_C begin at residue 467 and 539, respectively. LMM_C contains two minor species which start at 465 and 535, respectively. The N-terminal sequence of rod is LKKAETEK..., identical to that of S-2 which confirms that S-2 has the same N-terminus as rod. Our results suggest that the susceptible sites in the neck region are restricted to a narrow region whereas those at the S-2/LMM joint are dispersed within a much larger area (Supported by NIH and AHA).

T-AM-E8 FROM MYOSIN RODS TO MYOFIBRILS: EFFECTS OF MG^{2+} ON CROSS-BRIDGE ORIENTATION AND MYOSIN ASSEMBLY. E. Reisler, J. Liu* and P. Cheung*, Department of Chemistry and Biochemistry and the Molecular Biology Institute, UCLA, Los Angeles, CA 90024.

Chymotryptic digestion of myosin rod filaments in the pH range 7.0-8.2 proceeds at two major sites. The initial cleavage near the N-terminal end of the molecule (site 1) produces shorter rods (by 10K) and is followed by proteolysis at the LMM/S-2 junction (site 2). At pH 8.0 both digestion sites are protected by mM levels of Ca^{2+} or Mg^{2+}, but only site 1 is affected by MgADP and MgATP. The effect of divalent cations on digestion of rod filaments is pH-dependent, and it results in dramatically reduced pH-dependence of proteolysis at the LMM/S-2 junction. Light scattering measurements reveal a parallel "disensitization" of myosin and rod filament sizes to variations in pH (7.0-8.2). Cross-linking experiments show that mM concentrations of divalent cations reverse the alkaline pH-induced release of myosin cross-bridges. The same mechanism appears to operate in myofibrils as evidenced by their chymotryptic digestions in the presence of 5mm Mg^{2+} in the pH range 7.0-8.2. This research was supported by grants from MDA and USPHS (AM 22031).

T-AM-E9 MELTING OF S-2 AND CROSS-BRIDGE MOVEMENT D. Applegate and E. Reisler, Department of Chemistry and Biochemistry and the Molecular Biology Institute, UCLA, Los Angeles, CA 90024

Recent investigations by Harrington and collaborators have demonstratred that the rates of cross-linking the S-1 and S-2 regions of myosin to the thick filament surface decrease over a narrow pH range from 7.4 to 8.0 (e.g. Ueno & Harrington, J. Mol. Biol. (1981) 149, 619-640). Over the same pH range there is a sharp increase in the rate of proteolysis at the LMM-HMM junction. These results are consistent with charge induced release of myosin cross-bridges from the thick filament surface. In this study we employed myosin and rod minifilaments to examine directly whether conformational changes in the S-2 segment accompany the release of cross-bridges from the filament backbone. We prepared myosin and rod minifilaments at pH 7.0 and 8.0. The pH 7.0 species are morphologically similar to their pH 8.0 counterparts. Cross-linking experiments and proteolytic digestions of myosin and rod minifilaments demonstrated that these structures undergo similar pH induced changes in the rates of S-2 cross-linking and hinge digestion as previously observed with synthetic myosin filaments, myofibrils, and rod filaments. Circular dichroism studies reveal that at pH 8.0 the rod and myosin minifilaments have reduced α-helical content by 9 and 5% respectively, compared to the pH 7.0 structures. These changes are consistent with partial melting in the S-2 region of the molecule. This work was supported by an MDA post-doctoral fellowship and grants from USPHS(22031) and MDAA.

T-AM-E10 SELF-ASSOCIATION OF A SUBFRAGMENT-2 OF MYOSIN INDUCED BY DIVALENT METAL IONS. Hitoshi Ueno, Michael E. Rodgers and William F. Harrington. Department of Biology, The Johns Hopkins Univ., Balto., MD 21218.

The effect of divalent cations on the self-association of long S-2 and short S-2 fragments of rabbit skeletal muscle has been investigated. In the presence of millimolar concentrations of Ca^{2+} or Mg^{2+} long S-2 associates at neutral pH (μ = 0.06) to form ordered high molecular weight aggregates whereas short S-2 does not. The association process is cooperative and results from binding of 2-4 divalent cations within the C-terminal hinge region of long S-2. The aggregates could be detected by turbidity measurement and phase contrast light microscopy, and optical diffraction analysis of electron micrographs of the aggregates revealed 143 and 286 Å periodicities. Chymotryptic digestion studies of synthetic rod filaments revealed that proteolytic cleavage within the LMM/S-2 hinge was suppressed by Ca^{2+} or Mg^{2+} (<10 mM) at both pH 7 and 9 (μ = 0.13). These results suggest that the crossbridges exist in either an attached (A) or detached (B) state with respect to the thick filament surface and that the equilibrium between these two states is shifted towards the (A) state through binding of divalent cations in the HMM-LMM hinge domain. Thus our results provide evidence for the presence of low affinity divalent cation binding sites specifically localized in the HMM-LMM hinge domain in addition to the well-documented high affinity sites in the DTNB light chains. They suggest that binding of Mg^{2+} within the hinge domain under physiological conditions may act to lock the crossbridge to the thick filament surface in its resting state orientation.

T-AM-F1 FACTORS INFLUENCE CAFFEINE-INDUCED Ca^{2+} RELEASE FROM ISOLATED SR. J.Y. Su and W. Hasselbach, Dept. Anesthesiol. Univ. Wash. Seattle, Wa. 98195 and Max-Planck Institute Dept. Physiol. Heidelberg, FRG.

Reports on caffeine-induced Ca^{2+} release from isolated SR are equivocal suggesting that the conditions for its Ca^{2+} releasing action are not well understood. To explore the possible mechanism of caffeine action on the SR we have studied the effects of several factors (ATP, Mg, Ca, and ionic strength (μ)) on the caffeine-induced Ca^{2+} release from isolated SR. The SR (5000 xg) were prepared from rabbit skeletal muscle as described by de Meis and Hasselbach (1971). 0.2 mg/ml SR were loaded with ^{45}Ca (0.02 mM) to 96 ± 0.5 nmol/mg. We found that there was an immediate Ca^{2+} release in < 5 sec and a complete reuptake after 5 min. The caffeine dose-response curves were shifted to the left with increasing μ (0.08, 0.15 & 0.3) (at 0.5 mM caffeine, a net release of 2.5, 9 & 16 nmol Ca/mg respectively). The maximal Ca^{2+} release was smaller at μ 0.3 than that of the lower μ. The caffeine-induced Ca^{2+} release were qualitatively the same at μ 0.08 & 0.15 under various conditions: (1) It was a direct function of $[ATP_f]$ and $[Ca^{2+}_f]$ up to 3 μM), (2) at the initial release it was not changed by $[Mg^{2+}_f]$ (0.2-7 mM) and slightly decreased with increase in $[Mg^{2+}_f]$ at 15 & 30 sec, and (3) EGTA inhibited the initial release in a direct function of $[Ca^{2+}]$ but the release was increased after 3 min in a direct function of [EGTA]. We conclude that the optimal caffeine-induced Ca^{2+} release is at μ 0.15, $[Ca^{2+}_f]$ μM, and [ATP] > 0.5 mM. Supported by NIH HL 20754, RCDA and MPI fellowship.

T-AM-F2 MAMMALIAN PEELED MUSCLE FIBERS: CA2+ RELEASE IS GRADED BY Cl^- AND BLOCKED BY OUABAIN. Sue K. Donaldson, Department of Physiology and Department of Medical Nursing, Rush University, Chicago, Illinois 60612

In an earlier study (Biophys. J. 37:23a, 1982) an ouabain-sensitive component of Cl^- stimulated Ca^{2+} release in peeled (sarcolemma removed) rabbit skeletal fibers was demonstrated. Abrupt substitution of Cl^-, a membrane permeant anion, for an impermeant anion, such as propionate, stimulates release of Ca^{2+} from peeled fibers, presumably by depolarization of any sealed-off membrane systems, such as sarcomplasmic reticulum (SR) or transverse tubules (TT) within the peeled fiber. Osmotic effects were limited by concurrent substitution of choline for K^+ which kept $[K^+]x[Cl^-]$ a constant during Cl^- substitution. Ca^{2+} release was monitored as an isometric tension transient. The finding that part and sometimes all of this Cl^- stimulated release of Ca^{2+} was prevented by soaking the fibers in a 1mM ouabain solution for 2-3 hours prior to peeling, suggested that Cl^- acted on sealed-off polarized TT's within the peeled fiber. The caffeine stimulated release was unaltered by ouabain. Since Cl^- stimulation of the ouabain-sensitive component ultimately leads to Ca^{2+} release from the SR, this stimulation may involve the physiologic mechanism of TT depolarization governing SR Ca^{2+} release. In this study we find that varying the level of Cl^- stimulation grades the Ca^{2+} release of the ouabain-sensitive component, just as would be expected if stimulation were occurring via a physiologic TT-SR mechanism. Supported by grants from Muscular Dystrophy Association of American and NIH(HL23128, AM31511).

T-AM-F3 STIMULATION OF ^{45}Ca RELEASE IN SKINNED MUSCLE FIBERS BY SUSTAINED ION GRADIENTS. Elizabeth W. Stephenson, Dept. of Physiology, UMDNJ-NJ Med. Sch., Newark, NJ 07103

Depolarization of skinned twitch fibers by transfer from K propionate to KCl solution transiently stimulates a highly Ca^{2+}-dependent ^{45}Ca efflux, and might also inhibit SR Ca reaccumulation (J. Gen. Physiol. 71:411, 1978). The present studies examined ^{45}Ca release after Cl replaced the much less permeant anion methanesulfonate (MeS) at either constant $[K^+]$, or constant $[K^+][Cl^-]$ product wherein imposed gradients should dissipate slowly. ^{45}Ca efflux and isometric force were measured as described previously on segments of frog semitendinosus fibers skinned by microdissection. EGTA was added a few s after Cl (interrupted response), to minimize reaccumulation, or preceding Cl (pretreated response), to evaluate Ca^{2+} dependence. After KCl replaced KMeS, mean ^{45}Ca release in 1 min was 65% in interrupted responses, 27% in 5 mM EGTA-pretreated responses, and 19% in 10 mM EGTA-pretreated responses. After 120 mM choline Cl + 2.5 mM KMeS replaced 120 mM KMeS + 2.5 mM choline Cl, mean ^{45}Ca release was 34% (11) - 28% (15) in the variable, slower, interrupted responses, and 9.5% in 5 mM EGTA-pretreated responses, which was significantly larger than 5.3% control loss in 5 mM EGTA KMeS; in paired data from 6 fibers, stimulated release (above control) in interrupted responses correlated well with that in pretreated responses, with slope 8. When EGTA was added long after choline Cl, force remained elevated and ^{45}Ca release did not differ significantly from that in interrupted responses. These results suggest that depolarization at constant ion product stimulates a small Ca^{2+}-insensitive efflux that grades a larger Ca^{2+}-dependent flux, while KMeS to KCl also stimulates an osmotic component with low Ca^{2+} dependence; they are consistent with inhibition of reaccumulation by depolarizing gradients. Supported by Foundation of UMDNJ Grant 28-82 and NIH AM30420.

T-AM-F4 SPONTANEOUS CALCIUM RELEASE FROM SARCOPLASMIC RETICULUM. P. Palade and R. D. Mitchell. Dept. of Molecular Biology, Vanderbilt University, Nashville, TN 37235. (Intr. by F. W. Banks).

Rabbit skeletal muscle SR, preloaded with Ca^{++} in the presence of 112.5 mM phosphate, 1 mM MgATP and an ATP regenerating system, undergoes a rapid spontaneous Ca^{++} release following a 1-2 min lag after Ca^{++} uptake has been completed (Ca^{++} < 0.1 μM). Release is followed by reuptake and renewed release. Unidirectional Ca^{++} influx is reduced during and after a release. Both Ca^{++} release and unidirectional Ca^{++} efflux rates are dependent on the extent of Ca^{++} preloading and are inhibited by Ca^{++}_o in the 1-10 μM range if 1) the Ca^{++} pump is operative, 2) the Ca^{++} is added prior to the onset of release and 3) the pCa levels are maintained. Quercetin does not block release and removes the inhibition by Ca^{++}_o. Release rates as high as 10-20 μmol/mg·min have been recorded in the presence of 100 μM quercetin. Arrhenius plots of release rates demonstrate a break near 30°C, with Ea ∿ 25 Kcal/mol below 30°C. Mg^{++}, Mn^{++} and Sr^{++} are inhibitory to spontaneous Ca^{++} release, with Mn^{++} inhibiting from the outside and Sr^{++} from the inside of the vesicles. Rapid release requires phosphate in high concentrations, and other precipitating anions interfere. Influences of other anions and monovalent cations have also been noted. Spontaneous release is favored at pH 6.8-7.3 and inhibited by alkalinization after preloading. Additions of salt solutions during the lag period suggest that inside + potentials (SR "hyperpolarization") may increase the rate of subsequent spontaneous Ca^{++} release. Sucrose does not block the release, nor is sucrose released together with Ca^{++} (no membrane rupture). Spontaneous Ca^{++} release thus displays features distinct from Ca^{++}-induced, alkalinization-induced, and "depolarization"-induced Ca^{++} release. (Supported by NIH (AM 14632) to S. Fleischer).

T-AM-F5 EFFECT OF LOCAL ANESTHETICS ON SPONTANEOUS CALCIUM RELEASE FROM SARCOPLASMIC RETICULUM. P. Volpe, P. Palade, B. Costello and R. D. Mitchell, Department of Molecular Biology, Vanderbilt University, Nashville, TN 37235.

Several local anesthetics (tertiary amines, quaternary amines and neutral) were found to inhibit spontaneous calcium release from purified light SR (see Palade and Mitchell, Biophys. J., this issue). In the range of anesthetic concentrations used, Ca^{++} uptake generally was unaffected. With short preincubations, QX 572 (membrane permeant despite being charged) but not QX 314 (charged and membrane impermeant) significantly inhibited Ca^{++} release. In addition, by extending the preincubation period, a time-dependent increase in inhibition of Ca^{++} release by all the drugs tested was observed. These findings suggest that the receptor(s) for local anesthetics is situated on the internal side of SR vesicles. Studies of inhibition of unidirectional Ca^{++} efflux showed that more hydrophobic anesthetics actually took longer to reach equilibrium which may suggest that local anesthetics must dissociate away from the membrane in order to reach the internal receptor. Potency at equilibrium spanned about three orders of magnitude, with SKF 525-A, a tertiary amine, being the most effective (K_d ∿ 40 μM) Agents known to selectively inhibit permeability pathways for anions or monovalent cations did not inhibit spontaneous Ca^{++} release. Protonophores had no effect on the Ca^{++} release pattern whether local anesthetics were present or not. The latter findings suggest that local anesthetics interact directly with a Ca^{++} channel rather than with other permeability mechanisms that might indirectly influence Ca^{++} channel gating under other conditions. (Supported by NIH (AM 14632) to S. Fleischer).

T-AM-F6 KINETIC RESOLUTION OF THE COMPONENTS INVOLVED IN CA RELEASE FROM SARCOPLASMIC RETICULUM. Do Han Kim and Noriaki Ikemoto. Department of Muscle Research, Boston Biomedical Research Institute, and Department of Neurology, Harvard Medical School, Boston, MA. 02114

Release of Ca^{2+}, which had been accumulated in a heavy fraction of rabbit skeletal muscle sarcoplasmic reticulum in the presence of 0.5 mM Mg.ATP and of an ATP-regenerating system, was triggered by several different methods: a) an increase of extravesicular [Ca^{2+}] from about 0.1 μM to 10 μM, b) addition of caffeine (e.g. 2 mM) or quercetin (e.g. 70 μM), and c) substitution of K^+ for $choline^+$ to produce membrane depolarization. The time courses of rapid Ca^{2+} release (5--25 nmol Ca^{2+}/mg protein/s) were monitored by the stopped-flow spectrometry of the extravesicular [Ca^{2+}] with Arsenazo III. Addition of 20 μM dantrolene sodium produces selective inhibition of Ca^{2+} release induced by caffeine. However, addition of 1 μM ruthenium red or an increase of the extravesicular [Ca^{2+}] to > 10 μM inhibits all types of Ca^{2+} release induced by methods a, b and c. These results suggest that the Ca^{2+} release machinery consists of at least two sets of components: one set contains several receptors for different triggering signals that are distinguishable by selective inhibitors (e.g. dantrolene sodium); and the other, the Ca^{2+} channels that are blocked by common inhibitors regardless of the triggering methods (e.g. ruthenium red and high [Ca^{2+}]). (Supported by grants from NIH and MDA).

T-AM-F7 COMPUTER MODELING OF THE Ca^{2+}-Mg^{2+}-ATPase PUMP OF SKELETAL SARCOPLASMIC RETICULUM
Duncan H. Haynes, Dept. of Pharmacology, Univ. of Miami School of Medicine, Miami, Fl.

A mathematical model of the Ca^{2+}-Mg^{2+}-ATPase pump is presented. As pictured, the model describes the enyzme in terms of occupation of three sites: (a) A Ca^{2+}, K^+ and H^+ binding site, (b) an ATP/ADP binding site and (c) a phosphorylation site. Steady-state rates and concentrations of intermediates are calculated from input rate (and equilibrium) constants, and reactant and product concentrations. The computations are made on a DEC 1103 computer using matrix algebraic methods. The computations require no simplifying assumptions; the input rate constants are systematically varied to conform the model to the data. Simulations include the dependence of the initial rate on $[Ca^{2+}]_o$, $[K^+]$, $[Mg^{2+}]$, [Pi], $[Ca^{2+}]$, [ATP]/[ADP] ratio and pH. The model also predicts the correct dependence of the level of phosphoenzyme on these concentrations.

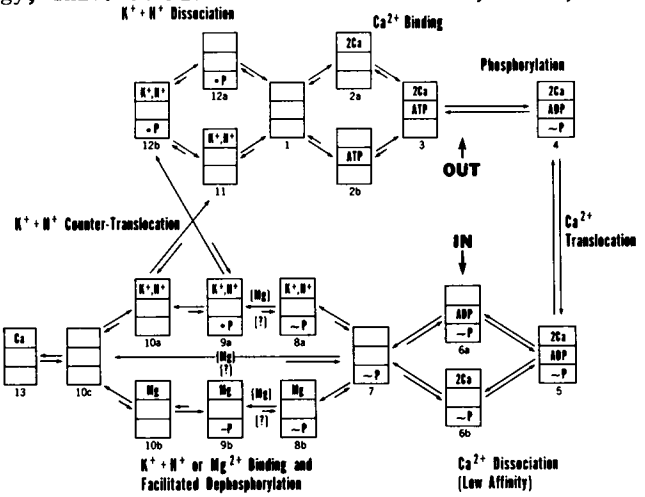

T-AM-F8 EXPLORING THE ADENINE NUCLEOTIDE BINDING SITE OF THE CA+MG ATPase FROM SARCOPLASMIC RETICULUM WITH PHOTOAFFINITY PROBES. Micahel B. Cable, John J. Dallara, and F. Norman Briggs, Medical College of Virginia, Richmond, VA 23298.

Three adenosine triphosphate (ATP) analogs were evaluated for their effectiveness as photoaffinity probes for the Ca+Mg-ATPase of sarcoplasmic reticulum (SR-ATPase): 8'-azido adenosine triphosphate (8-N_3-ATP), 3'-O-{3-[N-(4-azido-2-nitrophenyl)amino] proprionyl} adenosine triphosphate (aryl-N_3-ATP), and 3'-O-(4-benzoyl)benzoyl adenosine triphosphate (BZ-ATP). 8-N_3-ATP was a good substrate for the SR-ATPase with an apparent Km similar to that of ATP. However, photolysis with 0.1 to 2mM 8-N_3-ATP produced only minimal inhibition of ATPase rate (25% at 2mM 8-N_3-ATP) and low levels of analog incorporation. Photolysis of Aryl-N_3-ATP did not produce inhibition of ATPase activity at concentrations as high as 2mM. ATPase activity was depressed by the short wavelength ultraviolet light used to generate the active nitrenes. Due to these difficulties and the lack of photodependent inhibition by these compounds, the two azido derivatives were judged to be unsatisfactory as photoaffinity probes for the SR-ATPase. Photolysis of BZ-ATP by long wavelength light (λ 330nm) produced covalent incorporation of the analog and loss of ATPase activity. Fifty per cent inhibition was obtained with 200 to 500 μM BZ-ATP. Addition of the detergent $C_{12}E_8$ did not increase the level of inhibition. Polyacrylamide gel electrophoresis of the Ca+Mg-ATPase photolyzed with [^{3}H]-BZ-ATP showed labelling of a single protein band with the same R_f as Ca+Mg-ATPase. On the basis of these results, BZ-ATP was judged to be an effective photoaffinity analog of ATP.

T-AM-F9 SELECTIVE SPIN-LABELING OF THE CALCIUM PUMP PROTEIN (CPP) OF SARCOPLASMIC RETICULUM (SR). J. Oliver McIntyre and Sidney Fleischer. Department of Molecular Biology, Vanderbilt University, Nashville, TN 37235.

The CPP is the predominant membrane protein in the SR membrane. We have labeled the CPP in either the hydrophilic or hydrophobic domain using two selective spin-labeling reagents: 1) 4-maleimido-2,2,6,6-tetramethylpiperidinoxyl (Mal-SL6); or 2) N-cyclohexyl-N'(2,2,6,6-tetramethylpiperidinoxyl)-carbodiimide (NCCD). The Mal-SL6 and NCCD spin-labels are incorporated to ~1 mol/mol CPP with retention of ~65% and ~80% of the Ca^{2+}-pumping, respectively. The pumping efficiency remained constant at ~0.9 equiv. Ca^{2+} uptake/mol ATP hydrolyzed under the conditions of assay. The EPR spectrum of Mal-SL6-CPP exhibited a single spectral component with hyperfine splitting of 68G at 5°C and 66G at 25°C. The saturation transfer (ST)-EPR spectra of both Mal-SL6-CPP and NCCD-CPP exhibit anisotropic motional characteristics. The low field and high field parameters (L"/L and H"/H) did not show marked variation with temperature from 5°C to 35°C with τ_{appt} of about 10^{-4} sec, calibrated using hemoglobin as isotropic model for the motion. By contrast, the centerfield parameter (C'/C) was more sensitive to temperature with (τ_{appt} ~10^{-5} sec). Different conditions for incorporating the Mal-SL6 resulted in ST-EPR spectral features which appeared less indicative of anisotropic motion, i.e., L"/L and H"/H were more sensitive to changes in temperature and C'/C was less temperature sensitive. The EPR and ST-EPR spectra of both Mal-SL6-CPP and NCCD-CPP indicate that the motional characteristics of the spin-labeled CPP reflect the motion of the CPP within the membrane, which is approximately three orders of magnitude slower than the motion of the lipid in the membrane. [Supported by NIH 21987].

T-AM-F10 COOPERATIVE INTERACTIONS BETWEEN Mg^{2+} BINDING SITES ON SARCOPLASMIC RETICULUM. Stefan R. Highsmith. Department of Biochemistry, Univ. of the Pacific, San Francisco, CA 94115.

Tb^{3+} binding to SR vesicles and detergent-solubilized CaATPase was monitored by ATPase activity and fluorescence enhancement. Activity loss indicated a site with $K_{app} \geq 3 \times 10^6$ M^{-1}. Neither Ca^{2+} ($\leq$ 0.5 mM) nor Mg^{2+} ($\leq$ 20 mM) protected against inactivation. Activity was restored by EGTA. No Tb^{3+} fluorescence enhancement was observed for binding to this site.

Tb^{3+} fluorescence was enhanced about 950-fold by binding to 2 classes of sites, which were independent or negatively cooperative, as determined by Scatchard analysis. The K_{app} were 3.2×10^4 M^{-1} and 0.65×10^4 M^{-1}. Ca^{2+}($\leq$ 1 mM) had no affect. Mg^{2+} was a competitive inhibitor; K_{Mg}=94 M^{-1} in 10 mM MOPS, pH 7.0, 25°C. When SR was solubilized in 20 mg/ml $C_{12}E_9$ (Murphy, et al (1982) JBC 257,3551) 5 mM $MgCl_2$, 10 mM MOPS pH 7.0 and 1 mM EGTA, Tb^{3+} titration indicated a single class of sites with $K_{app}=5 \times 10^4$ M^{-1}. If EGTA was replaced by 0.1 mM Ca^{2+}, Tb^{3+} titrations indicated positive cooperativity between the sites. The total number of sites was constant. Mg^{2+} was still a competitive inhibitor.

These results indicate that there are two classes of Mg^{2+} binding sites on SR CaATPase vesicles which interact with one another. This interaction is modulated by Ca^{2+} and detergent. For Tb^{3+} binding to these Mg^{2+} sites, there seems to be negative cooperativity in SR vesicles, which is changed to positive cooperativity by $C_{12}E_9$ plus Ca^{2+}, or is lost by $C_{12}E_9$ minus Ca^{2+}. Preliminary data suggest the cooperativity loss is due to subunit dissociation. (NIH Grant AM 25177)

T-AM-F11 EFFECTS OF PHOSPHOLIPASE C ON THE Na^+-Ca^{2+} EXCHANGE AND Ca^{2+} PERMEABILITY OF CARDIAC SARCOLEMMAL VESICLES. Kenneth D. Philipson and Joy S. Frank. UCLA School of Medicine, Los Angeles CA 90024

We have examined the effects of phospholipase C pretreatment on Ca^{2+} transport in highly purified canine cardiac sarcolemmal vesicles. Na^+-Ca^{2+} exchange, measured as Na_i^+-dependent Ca^{2+} uptake, is stimulated by ~50% when 10-60% of the membrane phospholipid has been hydrolyzed. Although the phospholipase C treatment also increases sarcolemmal passive Ca^{2+} flux, the membrane maintains enough of a permeability barrier for enhanced transport (via Na^+-Ca^{2+} exchange) to be observed. These effects can be obtained with either phospholipase C from C. perfringens or B. cereus. We find that the phospholipase C (C. perfringens) is preferentially hydrolyzing phosphatidylcholine, phosphatidylethanolamine, and sphingomyelin leaving the negatively charged phospholipids, phosphatidylserine and phosphatidylinositol, intact. This suggests that the presence of negatively charged phospholipids is sufficient to ensure Na^+-Ca^{2+} exchange activity. Thin-section electron microscopy reveals gross morphological changes in phospholipase C-treated sarcolemma. The vesicles are aggregated and diacylclycerol droplets are visible. It is surprising that vesicles displaying severe structural damage can demonstrate enhanced transport activity. (Supported by NIH grant #HL 27821)

T-AM-G1 ASPARTATE TRANSCARBAMOYLASE FROM *E. COLI*: Zn^{2+} BONDING DOMAINS. A. Ginsburg, J. B. Hunt, S. H. Neece, and H. K. Schachman, NHLBI, NIH, Bethesda, MD 20205

Aspartate transcarbamoylase (ATCase) from *E. coli* contains 6 catalytic (c) chains and 6 regulatory (r) chains; the 4 -SH groups of each r chain are involved in tetrahedral bonding of Zn^{2+} at the c:r contact region (Monaco *et al.*, Proc. Natl. Acad. Sci. U.S.A. 75, 5276, 1978). Mercurials dissociate ATCase (Gerhart & Schachman, Biochemistry *4*, 1054, 1965). The release of Zn^{2+} from ATCase and from isolated r subunit, upon challenge by p-hydroxymercuriphenylsulfonic acid (PMPS), and the rebinding of Zn^{2+} by these proteins, upon displacement of PMPS with 2-mercaptoethanol (ME), have been studied using the sensitive, high-affinity metallochromic indicator 4-(2-pyridylazo) resorcinol at pH 7. When the -SH group of each c chain is protected, one Zn^{2+} is released for each four eq of PMPS added to ATCase during titration of the 24 -SH groups of r chains. Up to 4 PMPS/ATCase, the release of Zn^{2+} is pseudo-first-order and is virtually independent of [ATCase]. Stopped-flow traces for the reaction of ATCase with excess (0.1-1 mM) PMPS show a lag period followed by pseudo-first-order release of Zn^{2+} and the reaction order in [PMPS] $\simeq$ 1.4. Isolated r subunits that are competent to associate with c trimers to reconstitute ATCase bind Zn^{2+} with $K'_A > 10^7\ M^{-1}$ (presumably as r dimers). However, Zn^{2+} release produced by excess PMPS is > 3000-fold faster for r subunits than for ATCase. The rebinding of Zn^{2+} to r subunits, initiated by the rapid removal of PMPS with excess ME, is first-order in [Zn^{2+}] and first-order in [r chain] with an apparent second-order $k \simeq 10^5\ M^{-1}s^{-1}$ at 15°C. This second-order k is increased < 2-fold by the presence of c trimers, although in this case a rapid assembly of ATCase occurs. Thus, the rate limiting step in the assembly of ATCase could be Zn^{2+} binding to r dimers.

T-AM-G2 T4 TAIL FIBER TACTOIDS: STRUCTURAL ANALYSIS BY ELECTRON MICROSCOPY AND OPTICAL DIFFRACTION, Patricia Arscott*, Walter Runge†, and Victor Bloomfield*, *Department of Biochemistry, †Department of Laboratory Medicine and Pathology, University of Minnesota.

T4 tail fibers, like myosin and collagen, form spindle-shaped aggregates called tactoids under certain conditions of pH and ionic strength. These tactoids are several microns long, and about 100 nm across at their widest point. Individual tail fibers are visible at the tapered ends. Negatively stained tactoids have a distinct pattern of light and dark bands running transverse to the long axis and repeating every 116 nm. Each repeating unit contains 22 light bands symmetrically arranged about a midpoint, with spacings ranging from 3.9 to 8.6 nm. Preliminary data obtained by optical diffraction indicate that the tail fiber is longer than the repeating unit in the tactoid. Measurement of the smallest meridional spacing in the diffraction pattern gives a length of 170 nm, in close agreement with a previous report that the distal half-fiber alone is 81.5 nm long [Earnshaw et al. (1979) J. Mol. Biol. 132: 101]. We therefore infer that the tail fibers overlap substantially in forming the tactoid. Each repeating unit is also characterized by a bulge in the middle which indicates the probable position of the kink in the fiber (the juncture of proximal and distal half-fibers). Measurement of the cross angle in the diffraction pattern shows that the fibers are out of parallel register by 7.73 deg. The included angle between proximal and distal half-fibers is therefore 164.5 deg. The optical diffraction pattern is being further analyzed for details of the packing arrangement of the tail fibers in the tactoids and the fine structure of individual fibers.

T-AM-G3 THEORY OF THE NUCLEATION CONTROL OF SICKLE HEMOGLOBIN POLYMERIZATION F.A.Ferrone (Dept. of Physics, Drexel University, Philadelphia 19104) J. Hofrichter and W.A.Eaton (Laboratory of Chemical Physics, NIADDK, NIH, Bethesda, MD 20205).

The self assembly of sickle hemoglobin polymers has been described as incorporating both homogeneous nucleation in bulk solution and heterogeneous nucleation onto the surface of preexisting polymers.[1] We present a simple statistical thermodynamic treatment of the kinetics of polymerization in this double nucleation model. This description quantitatively predicts all features of the kinetics as measured by a photolytic method in the region of 1 msec to 10 sec^1, as well as describing the behavior in the regime >10 sec extensively studied by temperature jump. For long delay times, the "supersaturation equation" arises explicitly.[2] We find that simpler treatments which neglect nonideality of monomer or nucleus, or models in which the nucleus sizes are fixed, fail to reproduce the data with physically reasonable parameters. This theory predicts a strong dependence of nucleus size on supersaturation. As concentration is varied from .19 to .39 g/cm^3 the homogeneous nucleus drops from 20 to 4, while the heterogeneous nucleus drops from 19 to 1. The variation in nucleus size results from a changing balance of entropy lost versus energy gained from bonds formed in the polymer. For the infinite polymer we find the loss in entropy from rigid body motion contributes 16 kcal/mol while the gain in binding energy is 12-14 kcal/mol (using a 1 mM standard state). This treatment predicts that homogeneous nucleation is an extremely rare event. For delay times above 10 sec almost all polymers are formed by the heterogeneous pathway, which alone determines the concentration and temperature dependence in that regime.

1/Ferrone et al, Biophys. J. (1980) 32,361 2/Hofrichter et al, PNAS (1976) 73,3035

T-AM-G4 ERYTHROCYTE NON-UNIFORMITY AND THE INTRACELLULAR POLYMERIZATION OF SICKLE HEMOGLOBIN. A.N. Schechter, D.A. Torchia and C.T. Noguchi. National Institutes of Health, Bethesda, Md.

We have previously reported the detection, by $^{13}C/^{1}H$ nuclear magnetic double resonance spectroscopy (NMR), of polymerized hemoglobin S in whole blood from sickle cell patients at high oxygen saturation (>90%). In order to study the relationship between the distribution of intracellular hemoglobin concentration and polymer formation, whole populations of SS, AS and SC erythrocytes were separated using discontinuous Stractan density gradients. For the SS erythrocytes, subpopulations with narrow ranges of intracellular concentrations (means from 29 to 42 g/dl) were isolated and the NMR was used to determine intracellular polymer as a function of oxygen saturation. The experimental results for each subpopulation agreed closely with theoretical predictions based on newly published data for cell-free hemoglobin solutions and a newly refined analysis of the non-ideal behavior of hemoglobin and water at intracellular concentrations. Indeed, from this analysis of the behavior of relatively homogenous subpopulations of sickle cells and from measurements of the density distribution we can now reconstruct the experimentally measured amount of polymer, as a function of oxygen saturation, for whole SS blood and determine the contribution of each fraction to intracellular polymerization. Recent work on the interactions of hemoglobin S with other hemoglobins and density gradient measurements on AS and SC cells (Bunn et al., PNAS, in press) also allow us to predict the measured polymer distribution of AS and SC cells. NMR measurements on AS and SC cells confirm this analysis. In general, cell non-uniformity further exaggerates the appearance, due to non-ideality, of hemoglobin S polymer at high oxygen saturation and suggests the particular importance of the very dense cells in the pathogenesis of the sickle hemoglobin syndromes.

T-AM-G5 SPECTRAL PROPERTIES OF THREE QUATERNARY ARRANGEMENTS OF *Pseudomonas* PILIN. Tania Watts, Cyril Kay and William Paranchych, Department of Biochemistry, University of Alberta, Edmonton, Alberta T6G 2H7.

Pili are filamentous appendages, distinct from flagella, found on the surfaces of bacteria. *Pseudomonas* pili are involved in such processes as bacterial adhesion, twitching motility and bacteriophage adsorption. The pili consist of a single type of protein subunit, pilin, arranged in a helix. The pili appear to be able to dissociate (retract) into the bacterial cell, thereby bringing attached bacteriophage in contact with the cell surface. Hence it is of interest to study the nature of the subunit/subunit interactions in pili in order to understand how this reversible assembly could occur. In this study the techniques of circular dichroism, solvent perturbation and absorption spectroscopy were used to probe the environment of aromatic amino acids in three forms of pilin, namely: native pili, pilin dimers in octyl-glucoside and in an *in vitro* assembled form of pili — 9 nm pilin filaments. The results showed that the region around tyr 24 and tyr 27 is buried at the subunit/subunit interface in native pili but becomes exposed upon dissociation of pili into dimers and that tyr 24 and 27 are partially buried in the 9 nm filaments.

(Supported by the Medical Research Council of Canada and the Alberta Heritage Foundation for Medical Research).

T-AM-G6 FRACTIONATION AND PRELIMINARY PHYSICAL AND CHEMICAL CHARACTERIZATION OF THE COMPONENTS OF HAGFISH SLIME GLAND MUCUS. Warren H. Gallagher and Victor A. Bloomfield, Department of Biochemistry, University of Minnesota, St. Paul, Minnesota 55108.

Pacific hagfish slime gland mucous vesicles isolated by the procedure of Downing et al. (1981 Science 214, 1143) are stable in solutions containing high concentrations of $(NH_4)_2SO_4$ or sodium salts of citrate, tartrate, or acetate. Upon dilution of the stabilizing salt, the vesicles release their contents, converting the solution to a clear mucous gel. The unfractionated mucus is composed of approximately 77% protein, 12% carbohydrate, 6% sulfate and 5% lipid by weight (Salo, personal comm.). The protein is strikingly high in proline (27%), serine + threonine (19%), and valine (14%). The carbohydrate has a high hexosamine content, as NAc-galactosamine and NAc-glucosamine, plus galactose and sialic acid. SDS-PAGE reveals that the protein components consist of a very high mol. wt. component, a predominant 52k dalt. component, and many additional components which migrate as 20k to 200k dalt. proteins. Except for the 52k component, the other lower mol. wt. components appear to be linked though disulfide bonds into large mol. wt. aggregates, and can be separated from the 52k component by gel permeation chromatography in 5M GuHCl. The gel state of the mucus can be disrupted by reduction of -S-S- bonds and by shear stress. The gel undergoes a reversible collapse upon addition of citrate, tartrate or acetate ions, a transition which leaves some of the 52k component in the solution phase. The lower mol. wt. components, after removal of the 52k component and reduction of -S-S- bonds, undergo an entropy-driven aggregation in the presence of citrate ion. This aggregation can be reversed by the addition of GuHCl. (Supported by NIH grant HL-24952 and a Cystic Fibrosis Foundation Research Fellowship to W.H.G.)

T-AM-G7 HYDRODYNAMICS OF MUCOUS GLYCOPROTEINS. Victor A. Bloomfield, Dept. of Biochemistry, Univ. of Minnesota, 1479 Gortner Ave., St. Paul MN 55108.

To understand how mucous glycoproteins, or mucins, confer such striking flow properties on mucous secretions, we must understand mucin structure. Although there is variation among mucins from different sources, the "bottlebrush" structure is a common motif. A typical mucin monomer has mol wt 5×10^5, 20% protein and 80% carbohydrate. About 25% of the polypeptide chain is unglycosylated or bare, while 75% is densely substituted with oligosaccharide chains, averaging about 8 sugar residues. Unless the mucins are treated with S-S reducing agents, proteases, and denaturants, they are usually found to have molecular weights around 2×10^6. Thus we model the normally occuring form as a tetramer, crosslinked like a star in the bare region. With this structural model, we confront published data with modern hydrodynamic theories to obtain a picture of mucin solution structure. For the oligosaccharide side chains, we used a treatment developed for partially porous spheres. For the composite structure of glycosylated and bare regions, we used subunit hydrodynamic theory. For the effects of branching, we used published theories for branched random coils and extended the broken-rod results of Wilemski to cover branched rodlike structures. The major conclusions are: (1) The glycosylated region is more like a random coil than a rigid rod. (2) The bare region is probably not highly extended. (3) Comparison of hydrodynamic properties of monomers and branched tetramers suggests that the monomer is more rigid in the tetramer. This may be due either to underestimation of aggregation in analysis of the experimental data, or to a real stiffening effect imposed by polyelectrolyte and steric repulsive interactions with the other chains in the branched mucin.

T-AM-G8 THE SOLUBILITY OF PARAMYOSIN AS A FUNCTION OF IONIC STRENGTH AT PH VALUES ABOVE AND BELOW THE ISOELECTRIC POINT. S. Krause and N. L. Munson, Dept. of Chemistry, Rensselaer Polytechnic Institute, Troy, NY 12181.

The solubility of paramyosin as a function of ionic strength (I) was measured at various pH values between 3.4 and 10.0. At each pH, I varied from 0.01 to 0.40 m. At pH 3.4, well below the isoelectric pH (5.9) of paramyosin, the protein was soluble at least up to 1 mg ml^{-1} up to I = 0.20 M, while < 0.1 mg ml^{-1} was soluble at I = 0.40 M. At pH 3.8 -3.9, the protein had a maximum solubility at an intermediate ionic strength, I = 0.05 M; this is akin to the "salting-in: salting out" effect that is generally expected with increasing I at constant pH. At all values of pH above the isoelectric pH, however, from pH 6.4 to 9.6, the protein had a minimum solubility at a value of I somewhere between 0.01 and 0.40 m. At pH 10.0, paramyosin was soluble at least up to 1 mg ml^{-1} at all values of I. A possible explanation for the difference in behavior above and below the isoelectric pH will be discussed; this explanation involves the difference in charge density on the protein in the pH range 3.4 to 3.9 versus that in the pH range 6.4 to 6.9.

It is postulated that three different processes contribute to the solubility of the protein: 1) a counterion adsorption process, decreasing the effective charge on the protein, which increases with increasing ionic strength and leads to diminished solubility with increasing ionic strength, 2) a "normal" "salting-in" effect which results in increased solubility with increasing ionic strength, and 3) a "normal" "salting-out" effect which results in diminished solubility when the ionic strength becomes high enough.

T-AM-G9 EXTENDED AND COLLAPSED CONFORMATIONS OF FIBRONECTIN DEMONSTRATED BY SEDIMENTATION AND ELECTRON MICROSCOPY. H. P. Erickson and N. Carrell. Anatomy Department, Duke University, Durham, NC 27710.

Plasma fibronectin consists of two identical polypeptide chains of 220,000 MW, joined by a disulfide bond near their carboxyl termini. Electron microscopy has shown the molecule to be a long flexible strand, 2 nm in diameter and 120 to 160 nm long (Erickson et al., J. Cell Biol. **91**:673). Alexander et al. (J. Biol. Chem. **254**:1501) reported that the sedimentaion coefficient increased from 10.8 S in 0.4 M KCl, to 13.6 S in 0.05 M KCl. We have confirmed these values for sedimentation in 15% to 40% glycerol gradients at 20° C. We have also studied half molecules of fibronectin, prepared by treatment with 2 mM DTT for 10 min (in 4 M urea, 0.2 M NaCl, 0.05 M tris, pH 8.5, 20° C), followed by 4 mM iodoacetamide. The half molecules had sedimentation coefficients of 7 S and 10 S in high and low ionic strength, respectively. The increase in sedimentation coefficient in low ionic strength implies that the molecule adopts a more compact conformation. Our results with half molecules suggest that the conformational change occurs within each half molecule. Electron microscopy of rotary shadowed specimens, prepared from high and low ionic strength, show the conformational change to be in the flexibility or folding of the thin strand. At high ionic strength the molecules were mostly well-extended strands, whereas at low ionic strength both whole and half molecules were kinked and bent to form more compact structures.

T-AM-G10 EARLY STAGE POLYMERIZATION OF E66 TMV PROTEIN. Ragaa A. Shalaby and Max A. Lauffer. Biophysical Laboratory, Dept. of Biological Sciences, University of Pittsburgh, Pittsburgh,PA 15260

As previously reported, the loading concentration, C, at which the first trace of 20S component appears in the ultracentrifuge has been used to investigate the effect of temperature, pH and ionic strength, μ, on the polymerization of TMV coat protein. From these measurements, ΔH, ΔS and ΔW_{el} per mole of A protein and the salting-out constant, K_s', were determined. The same procedure has now been followed for obtaining these parameters for the protein of E66, a mutant of TMV, differing only in the substitution of lysine for asparagine at position 140. This results in a less hydrophobic protein with one less net negative charge per subunit at pH 7. Prior to each sedimentation run, the protein at the desired pH, μ and concentration was warmed slowly to the desired temperature and incubated in the centrifuge at that temperature for at least 6 hours. To investigate the effect of μ, experiments were carried out at 12°C and pH 6.7 with values of μ between 0.01 and 0.15. For studying the effect of temperature, experiments were carried out at pH 6.7 and μ of 0.10. The effect of pH was determined by sedimentation measurements at constant T and μ. The results show that ΔH and ΔS and the binding of hydrogen ions are nearly the same as for the polymerization of TMV protein. However, the electrical work contribution, ΔW_{el}, and the salting-out constant, K_s', both determined from the effect of ionic strength, are each approximately one-half the values previously obtained for TMV protein, in nearly quantitative agreement with expectation from the difference in amino acid composition. This result provides strong support for the appropriateness of this method of analysis. (Supported by NIH Grant GM 21619.)

T-AM-G11 ION BINDING BY TMV, TMV PROTEIN AND TMV-RNA. Warren H. Gallagher, H. H. Gastfriend and Max A. Lauffer. Biophysical Laboratory, Dept. of Biological Sciences, University of Pittsburgh, Pittsburgh, PA 15260.

Calcium ion titrations were carried out on TMV and TMV coat protein and both calcium ion and potassium ion titrations on TMV-RNA using ion-specific electrodes. Scatchard analysis showed that near neutrality the virus has two Ca^{++} binding sites, treated as non-identical, independently titrating centers, with apparent stability constants, β_{Ca}', greater than 10^4 M^{-1}. The higher affinity site for TMV titrated in water has a value of $\log\beta_{Ca}'$ which varies from 8.5 at pH 8.5 to 3.9 at pH 5. For Ca^{++} titration of TMV in 0.01 M KCl, the value is between 6.2 at pH 8.0 and 3.7 at pH 5.5. The higher affinity site for TMV in water binds up to two competing H^+ ions, one with an apparent pK_H greater than 8.5 and the other with a value which varies from 6.0 at pH 5.5 to 7.3 at pH 8.0. For TMV in 0.01 M KCl, only the competing H^+ ion binding with pK_H greater than 8.5 remains. TMV coat protein is incapable of binding Ca^{++} under equilibrium conditions at pH values above its isoionic point, but they are bound under nonequilibrium conditions. RNA in water bound 0.45 Ca^{++} ions per nucleotide with an apparent stability constant of $\log\beta_{Ca}$ = 6.03. 0.24 H^+ ions were released per Ca^{++} bound. Less Ca^{++} was bound in 0.01 M KCl solution and no H^+ ions were released. K^+ titrations in water solution showed that this ion is bound to the extent of 0.25 per nucleotide with $\log\beta_K$ of 2.96 and very little H^+ released. These results explain the fact that TMV and polymerized TMV coat protein have identical electrophoretic mobilities. (Supported by NIH Grant GM 21619.)

T-AM-G12 STEM MASS MEASUREMENTS OF POLYOMA CAPSIDS AND VIRIONS. T.S. Baker, I. Rayment, D.L.D. Caspar and W.T. Murakami, Rosenstiel Basic Medical Sciences Research Center and Department of Biochemistry, Brandeis University, Waltham, MA and J. Wall and J. Hainfeld, Biology Department, Brookhaven National Laboratory, Upton, NY.

The unexpected discovery by Rayment et al. (Nature 295, 110, 1982) that the 72 capsomeres of the polyoma virus capsid are all pentamers shows that bonding specificity is not conserved among the protein subunits in this icosahedrally symmetric assembly. Physicochemical characterization of polyoma virus particles has been limited to a few studies, most tending to support the 360 subunit model revealed by X-ray crystallography. Electron scattering measurements on unstained, unfixed particles in the scanning transmission electron microscope (STEM) provide a unique procedure for measuring the molecular weight of individual particles and, thereby, the weight distribution of the population. Preliminary analysis of mass measurements of capsids (899 particles; M_r=16.1±1.4x10^6 daltons) and virions (440 particles; M_r=20.7±1.0x10^6 daltons) are in complete agreement with the 360 VP1 subunit model. The virion mass is about 10% lower than previously measured using physical-chemical methods. The possibility that this low value may result from systematic errors in the STEM measurements is being explored. Alternatively, the composition of the complete virion may be somewhat different than expected from other measurements. Examination of developmental intermediates, including minichromosomes, previrions and tubular polymorphic aggregates by STEM, conventional electron microscopy and image analysis techniques will provide more detailed information about their composition, interrelation and role in the control of virus assembly. Supported by NIH grant CA15468 (DLDC).

T-AM-G13 DIFFERENCES IN ISOTUBULINS IN NEONATE RAT AND HUMAN BRAINS. Deborah J. Field, Timothy R. Rustan*, William H. Frey* and James C. Lee. Dept. of Biochemistry, St. Louis University School of Medicine, St. Louis, MO. 63104 and St. Paul-Ramsey Medical Center, St. Paul, MN. 55101.

A high resolution two-dimensional gel technique was developed. It is capable of separating tubulin into 17-20 subspecies. Using this in conjunction with the one-dimensional isoelectric focusing technique, isotubulins in calf, human and rat brains were studied. Purified adult brain tubulin from these species can be resolved into 17 individual bands. Although the number of isotubulins appears to be conserved there are quantitative differences. In general, the distribution in bovine brain was very similar to the adult human brain samples tested. However, adult rat brain showed lesser amounts of the more basic β-tubulins.

Purified tubulin from neonate human and rat brain showed both quantitatively and qualitatively significant differences from the adult samples of the same species. In addition, the predominant isotubulin forms present in neonate brains are apparently dependent on the species. In the 3 day-old rat, the most significant change is in β-tubulin 11/12 which is found not to be resolved into β-11 and β-12 as in the adult rat and the most acidic β-tubulins, 15 to 17, are not detected. In the 11 day-old human brain, β-12 and β-14 are the predominant forms although all the other forms of β-tubulin can be detected in both the neonate and adult brains. The ratio of α to β tubulins is significantly lower in neonate human brain than in neonate rat brain.

T-AM-H1 INTERACTION OF MELITTIN WITH PHOSPHOLIPID MEMBRANES. S. Georghiou, G. N. Georgiades, and A. K. Mukhopadhyay, Biophysics and Chemical Physics Laboratory, Department of Physics, The University of Tennessee, Knoxville, TN 37996-1200

We have studied the interaction of melittin, the major protein component of bee venom, with distearoyl phosphatidylcholine bilayer liposomes by employing the enchancement of the 0 - 0 vibronic transition of pyrene, the formation of intramolecular excimers by 1, 3-bis-(1-pyrene) propane, and the nanosecond emission anisotropy of 1, 6-diphenyl- 1, 3, 5-hexatriene (DPH). Melittin is found to induce structural changes in the phospholipid which affect the ability of pyrene to penetrate into the bilayer. The effect is most pronounced in the vicinity of the T_t of the lipid. The protein affects the activation energy, E_a, for intramolecular excimer formation. Above T_t, E_a increases with increasing the melittin-to-lipid molar ratio reaching a value of 5·5 kcal/mol for 1:40 as compared to 3·1 kcal/mol in the absence of the protein. Below T_t, E_a increases only slightly from 10·5 kcal/mol in the absence of the protein to 11·6 kcal/mol for the above molar ratio. Protein effects on the kinetics of excimer formation have been followed by time-resolved emission spectroscopy on the nanosecond time scale. Nanosecond time-resolved emission anisotropy measurements, which allow the delineation of the effects of the protein on the order and on the dynamics of the hydrocarbon chains, have been carried out and the findings will be discussed.

T-AM-H2 CRYSTAL AND LIQUID CRYSTAL PACKING OF NONIONIC DETERGENTS UTILIZED FOR SOLUBILIZATION OF INTEGRAL MEMBRANE PROTEINS. D.L. Dorset, Med. Fndn. of Buffalo, Inc., Buffalo, NY 14203 and J.P. Rosenbusch, European Molecular Biology Laboratory, Heidelberg, West Germany.

Two classes of nonionic detergents, i.e. n-alkyl glucosides and n-alkyl oligo(ethylene oxide)s, are invaluable for the solubilization and purification of intergral membrane proteins such as the matrix porin from the outer membrane of *E. coli*. For the understanding of both detergent vesicle structure and the possible detergent aggregation in one crystal form of matrix porin, we have studied their solid state properties by electron diffraction, powder X-ray diffraction, differential thermal analysis and polarization optical microscopy. Anomeric forms of n-octyl glucoside(OG) exhibit distinct crystallization properties commensurate with their strikingly different water solubilities. The α-OG has more completely crystallized acyl chains at room temperature than does the βOG, which seemingly has a crystal packing similar to its methyl homolog. Near 70°C both anomers transform to a liquid crystalline state but only the α-OG is smectic. The βOG, in general, does not behave like a typical amphiphile, perhaps explaining its good water solubility. Alkyl ethers of oligo(ethylene oxide)s ($n\text{-}C_nE_m$) where n=8 or 12, crystallize with polyether moieties E_m in the stable poly(ethylene oxide) structure when $m \geq 4$. The alkyl chains are inclined to the polymer chain axis by 25° and pack in a methylene subcell similar to M||. Addition of water to these detergents gives an altered oligo(ethylene oxide) conformation quite unlike the solvent-stabilized extended chain found in hydrated poly(trimethylene oxide); the alkyl chains in the lyotropic liquid crystals are quite disordered. Supported by NIGMS GM21047, NSF DMR81-16318 & Swiss National Fonds Grant 3.656.80.

T-AM-H3 FIBRINOGEN BINDING TO HUMAN ERYTHROCYTES AND ENERGETICS OF ROULEAUX FORMATION, J. Janzen and D.E. Brooks, Dept. of Pathology, University of Brit. Col., Vancouver, Canada V6T 1W5

Fibrinogen binding to human erythrocytes (RBCs) has been implicated as the mechanism responsible for the cell/cell adhesions known as rouleaux. The binding to RBCs of purified, ^{125}I-labelled fibrinogen and the free energy of formation of RBC/RBC contacts have been estimated. The binding was estimated from the radioactivity in cell pellets produced by ultracentrifugation. The presence of free ^{125}I in such cell pellets constitutes an important artifact because ^{125}I can traverse the the cell membrane. The free label contribution to apparent binding was estimated from the change in apparent binding with cell concentration and from analysis of cell pellets subjected to serial washing. The measured binding at 1 mg/ml fibrinogen and 25°C is $\lesssim 250 \pm 60$ molecules/cell. The isotherm is apparently linear to 10 mg/ml. The adhesion energy was estimated (by the method of Evans and Buxbaum, Biophys. J. 34, 1-12, 1981) to be 3.6×10^{-3} erg/cm^2 ± 40% at 8.8 mg/ml fibrinogen. The implied fibrinogen surface binding energy is thus $\geq 32 \pm 16$ kcal/mole. Estimation of binding by measurement of radiolabel removed from solution does not require ultracentrifugation of cell suspensions. Although this method is not sensitive enough for systematic investigation of the low levels of binding encountered, the binding may be estimated to be < 2000 molecules/cell (1 standard deviation above zero) at 1 mg/ml. The surface binding energy in this case would be $> 4 \pm 2$ kcal/mole. Binding energies greater than 16 kcal/mole suggest covalent bonding and are thus at odds with the reversible nature of the observed RBC/RBC contacts. It is felt that the centrifugation procedure may be displacing, from the cell pellets, fibrinogen involved in the formation of the RBC/RBC contacts. Supported by the Medical Research Council of Canada.

T-AM-H4 BINDING OF CYTOTOXIC T-LYMPHOCYTES TO SUPPORTED LIPID MONOLAYERS CONTAINING TRYPSINIZED H-2K^k. Mamoru Nakanishi,* Adrienne A. Brian and Harden McConnell; Department of Chemistry, Stanford University, Stanford, CA 94305.

Products of the mouse major histocompatibility complex, H-2K and H-2D, are transmembrane proteins specifically recognized by cytotoxic T cells (CTL) either in conjunction with foreign antigens or alone in the course of graft rejection. We have incorporated H-2K^k into lipid monolayers supported on alkylated glass. Cloned CTL selected for high activity and specificity for H-2K^k bind specifically to these monolayers. Monolayers were made at an air-water interface, from lipid vesicles containing H-2K^k previously trypsinized to remove its intracellular portion. The monolayers were transferred to alkylated glass coverslips which were then attached to microscope slides. Cloned CTL were introduced between the cover glass and slide and allowed to settle onto the monolayer. Following incubation, the slide was inverted and examined with a microscope. We found that the percentage of cells remaining on monolayers containing H-2K^k increased as cell concentration decreased. At low cell concentrations the percentage of cells bound to these monolayers was significantly higher than the percent bound to control monolayers lacking H-2K^k. Preincubation of H-2K^k containing monolayers with alloantisera that block cytotoxicity reduced binding to levels seen with control monolayers, while treatment with normal mouse serum had no effect. Thus, this method offers the possibility of studying specific CTL adhesion to well defined model membranes in an orientation that allows direct observation of the contact region without the strong mechanical forces commonly employed in making T cell-target cell conjugates. *Permanent address: Faculty of Pharmaceutical Sciences, University of Tokyo, Bunkyo-ku, Tokyo, Japan.

T-AM-H5 GLYCOLIPID TRANSFER PROTEIN FROM BOVINE BRAIN. M. Wong, J.M. Vile, Y. Barenholz and T.E. Thompson, Department of Biochemistry, University of Virginia School of Medicine, Charlottesville, VA 22908.

Glycolipid transfer protein from bovine brain was purified partially by ammonium sulfate precipitation, CM52 ion exchange and Sephadex G75 column chromatography. Both pyrene and ^{3}H-labeled glucocerebroside were used to study the kinetics of transfer between donor and acceptor vesicles. Protein accelerated glucocerebroside transfer specifically; protein did not accelerate phospholipid transfer. The Sepharose CL2B column profile of donor and acceptor vesicles was not changed by protein. In colyophilized small sonicated vesicles (10% glucocerebroside, 90% 1-palmitoyl-2-oleoylphosphatidylcholine) about 2/3 glycolipid was transferred in 2 hours and the remaining 1/3 did not transfer (up to 5 hours). For donor and acceptor vesicles made of dipalmitoylphosphatidylcholine or 1-palmitoyl-2-oleoylphosphatidylcholine, glucocerebroside (10% in donors) was transferred only when both the donor and acceptor matrix phospholipids were in the liquid-crystalline state. [Supported by N.I.H. Grants GM-23573 and GM-14628].

T-AM-H6 SPONTANEOUS TRANSFER OF ASIALO GM1 BETWEEN PHOSPHOLIPID VESICLES. Rhoderick E. Brown and T.E. Thompson, Dept. of Biochemistry, University of Virginia, Charlottesville, VA 22908.

The kinetics of transfer of the neutral glycosphingolipid, asialo GM1, between phospholipid bilayers has been investigated by monitoring the movement of tritiated asialo GM1 from negatively-charged donor vesicles to neutral acceptor vesicles. The use of tritiated asialo GM1 (prepared by treatment with galactose oxidase and tritiated borohydride) has insured an unaltered glycolipid structure. Dipalmitoylphosphatidylcholine (DPPC) vesicles containing 10 mole % dipalmitoylphosphatidic acid (DPPA) and the tritiated asialo GM1 were incubated at 45°C with a ten or twenty fold excess of DPPC acceptor vesicles. Incubation aliquots were eluted through DEAE Sephacel minicolumns (0.7 cm x 2.5 cm) at various time intervals to separate the donor and acceptor vesicles. The net transfer of asialo GM1 to the neutral acceptor vesicles was calculated relative to that of ^{14}C-cholesterol oleate, which served as a nontransferable marker in the donor vesicles. Over ~36 hr at 45°C, the asialo GM1 transferred to the acceptor vesicles in a first order process. The half time of transfer was calculated to be ~412 hrs. (17.2 days) assuming that two thirds of the asialo GM1 was available for transfer from the donor vesicles and that no glycolipid flip-flop occurred. Varying the concentration of acceptor vesicles from a ten to twenty fold excess did not significantly alter the half time of transfer. These results are consistent with a mechanism involving transfer via the aqueous phase rather than a collisional complex between donor and acceptor vesicles. In addition, the extremely long transfer times of asialo GM1 are consistent with previous studies on other glycosphingolipids. [Correa-Freire, M.C., Barenholz, Y., and Thompson, T.E. (1982) Biochemistry 21, 1244-1248]. (Supported by USPHS grants GM-14628 and GM-23573).

T-AM-H7 PEPTIDES OF ERYTHROCYTE BAND 3 PROTEIN PRODUCED BY EXTRACELLULAR PAPAIN CLEAVAGE.
Michael L. Jennings, Mary Adams-Lackey, and Gerald H. Denney. Department of Physiology and Biophysics, The University of Iowa, Iowa City, Iowa 52242

Extracellular chymotrypsin cleaves human erythrocyte band 3 protein into two integral peptides of molecular weights 60,000 (CH60) and 35,000 (CH35); the cleavage has no effect on anion transport. Extracellular papain inhibits anion transport by lowering the rate constant for the efflux translocation step in the catalytic cycle for transport. The molecular basis for this inhibition is that papain cleaves CH35 into two integral peptides of molecular weights 30,000 (CH-P-30) and 5000 (CH-P-5). The latter peptide was not previously detected, but it can readily be visualized on gradient polyacrylamide gels run in the buffer system of Laemmli. CH-P-5 has been purified by two methods: preparative gel electrophoresis and Sephadex LH-60 chromatography in organic solvents. It contains no histidine and is rich in glycine. Preliminary end group analysis indicates that the alignment of the band 3 peptides is (CH60)-(CH-P-5)-(CH-P-30)-COOH. In chymotrypsin-treated cells, the stilbene disulfonate derivative H_2DIDS (4,4'-diisothiocyanodihydrostilbene-2,2'-disulfonate) can react covalently with both CH60 and CH35 to form a covalent cross-link between the two peptides. The site of the H_2DIDS covalent reaction with CH35 is on CH-P-30, if the H_2DIDS reaction precedes the papain cleavage. However, if the papain precedes the H_2DIDS, the H_2DIDS reacts preferentially with CH-P-5, forming a covalent cross-link between it and CH60. Therefore, the papain cleavage causes a rearrangement in band 3 such that an amino group on CH-P-5 becomes available for reaction with H_2DIDS, and the reaction with the amino group on CH-P-30 is occluded.
Supported by USPHS Grant GM 26861.

T-AM-H8 MOLECULAR THRESHOLD OF C5b-9 BINDING REQUIRED FOR ALTERED MEMBRANE PERMEABILITY,
Peter J. Sims, MD, PhD, Dept. of Pathology, Univ. of Virginia Med. Ctr., Charlottesville, VA.

The molecular threshold for formation of the complement lesion in human erythrocyte membranes has been determined by direct measurement of C5b-9 binding. C5b6, C7, C8 & C9 were isolated from human serum and assembled on resealed erythrocyte ghost membranes under non-lytic conditions. After C5b-9 assembly, sucrose-permeant ghosts were separated from sucrose-impermeant ghosts by density floatation. Analysis of ^{131}I-C8 and ^{125}I-C9 incorporated into membrane C5b-9 revealed:

(1) Formation of a sucrose-permeant pore in the erythrocyte membrane requires assembly of >300 C5b-9 complexes per cell, irrespective of the stoichiometry ($N \geq 1$) of C9 within each complex.

(2) When C9 is available in molar excess to bound C5b-8, a constant stoichiometry of 3 C9 bound per C5b-8 is observed for both sucrose-permeant and sucrose-impermeant cells.

(3) When C9 input is limiting (molar ratio of bound C9/C8<1), the threshold for pore formation increases as a hyperbolic function in membrane bound C5b-8. In the absence of C9, 11,700 C5b-8 complexes per cell are required to form a sucrose-permeant lesion in these membranes.

(4) Disulfide-linked C9 dimer is present in C5b-9 complexes isolated from both permeant and impermeant subpopulations of C5b-9 ghost membranes. Dimerization of C9 is shown to be catalyzed by free-SH groups on membrane proteins, in the absence of cellular or exogenous glutathione. These results suggest that transmembrane solute flow initiated by the C-proteins requires the interaction of multiple C5b-9 complexes bound to a single membrane, possibly mediated by C9 crosslinkages.
Supported by grants from AHA/VA Affiliate & Jeffress Memorial Trust. PJS is a John A. Hartford Fellow.

T-AM-H9 COMPOSITION OF THE INTERFACE MODULATES LECITHIN BINDING TO PHOSPHOLIPASE-A_2

C. D. DeBose and M. F. Roberts
Department of Chemistry, Massachusetts Institute of Technology, Cambridge, MA 02139

The binding of nonhydrolyzable ether-linked lecithin substrate analogues to cobra venom phospholipase-A_2 has been examined by multinuclear NMR and correlated with enzyme inhibition kinetics. Both the physical interactions and the kinetic effect of the dialkyl lecithins depend on the type of substrate matrix used. In simple two component dialkyl-/diacyl-lecithin systems (short-chain lecithin monomers or micelles and sonicated vesicles) the ether-linked compounds bind to the enzyme without Ca^{2+} and act as good inhibitors of lecithin hydrolysis. When the same combination of phospholipids is mixed with a detergent such as Triton X-100, Ca^{2+} becomes a prerequisite for lipid binding and the inhibition potency of the dialkyl lipids is dramatically decreased. Detergent induced changes in the characteristics of the interface are implicated in this effect.

The interaction of phospholipase-A_2 with sonicated vesicles of dihexadecyl phosphatidylcholine has also been examined by ^{1}H and ^{31}P NMR spectroscopy. When this enzyme binds to vesicles, it promotes loss of encapsulated lanthanide ions and appears to accelerate transbilayer "flip-flop" rates. These results have direct relevance to membrane asymmetry studies using phospholipase-A_2.

T-AM-H10 LIPID-PROTEIN AND PROTEIN-PROTEIN INTERACTIONS OF HUMAN MYELIN LIPOPHILIN. J.R. Silvius‡ G. Bruce Birell, J.M. Boggs,† P.C. Jost and O.H. Griffith, University of Oregon, Eugene, Ore., and †Hospital for Sick Children, Toronto, Ont. M5G 1X8

We have combined electron spin resonance (ESR) of lipid spin labels with high-sensitivity differential scanning calorimetry (HSDSC) to assess the extent and selectivity of phospholipid association with lipophilin from human myelin in reconstituted lipophilin/phosphatidylcholine (PC) bilayers. The number of lipids whose motion on the ESR time scale ($\sim 10^{-8}$sec) is influenced by each molecule of lipophilin, evaluated using a spin-labeled PC, increases as the lipid-to-protein ratio increases in the range 15-200 lipids per protein. This result is opposite to that expected if the motionally restricted component of the spin-labeled lipid's ESR spectrum arose only from lipid spin labels trapped in oligomeric complexes of the protein. As well, the number of lipids withdrawn from the cooperative phase transition by each lipophilin molecule (estimated by HSDSC) corresponds well with the number of lipids found by ESR to be associated with lipophilin in samples of various lipid-to-protein ratios. The observed decrease in the extent of lipid-protein association at higher bilayer concentrations of lipophilin is most readily interpretable as an oligomerization of the protein, with protein-protein contacts increasing at the expense of lipid-protein contacts, at higher lipophilin concentrations. Lipophilin associates preferentially with anionic spin-labeled lipids and associates less well with a cationic spin label than it does with PC. These results indicate that an appreciable portion ($\sim$ 25%) of the lipid-associating surface of lipophilin discriminates in favor of anionic lipids, in agreement with the results of previous calorimetric studies. (Supported by NIH Grant GM-25690).

T-AM-H11 THE ADDITIVITY OF BINDING ENERGIES FOR PHOSPHOLIPID-BOUND FACTOR V AND FACTOR V-DERIVED ACTIVATION PEPTIDES. Deborah L. Higgins and Kenneth G. Mann, Hematology Research, Mayo Clinic, Rochester, MN 55905

Bovine Factor V, the protein procofactor of the prothrombinase complex, is activated through limited proteolysis to form the active two subunit cofactor, Factor Va. The prothrombinase complex, which plays a critical role in the later stages of blood coagulation, is composed of the serine protease Factor Xa, the substrate prothrombin, Factor Va, Ca^{++} ions and a membrane surface (platelets *in vivo*). This complex can be modeled using purified proteins and phosphatidylcholine/phosphatidylserine vesicles. Factor V binds to phospholipid vesicles with $K_d = 4.3 \times 10^{-8}$ M, n = 214. The two activation intermediates (component B, M_r = 205,000 and component C, M_r = 150,000) both interact with phospholipids ($K_d = 1.8 \times 10^{-7}$ M, n = 140 and $K_d = 7.0 \times 10^{-7}$ M, n = 136, respectively). Through the use of the additivity of the Gibb's free energies, we determined that the binding interactions of these two components more than account for the binding of Factor V ($\Delta G^S < 0$). Isolated Factor Va (containing only the 74,000 dalton and 94,000 dalton subunits) also binds to phospholipid with a $K_d = 1.7 \times 10^{-7}$ M, n = 57. Only one of the two isolated subunits of Factor Va (component E, M_r = 74,000) binds to phospholipid ($K_d = 3.8 \times 10^{-7}$ M, n = 42). The component D subunit (M_r = 94,000) does not bind. The similarity between Factor Va and component E with respect to the dissociation constants and number of lipids (n) involved in binding one molecule of protein suggests that the binding energies of Factor Va quantitatively reside within the 74,000 dalton subunit. (Supported by HL-17430D and HL-07069 and by the Mayo Foundation)